REPORT DOCUMENTATION PAGE

Form Approved
OMB No. 0704-0188

1. REPORT DATE *(DD-MM-YYYY)*	2. REPORT TYPE	3. DATES COVERED *(From - To)*
28-02-2006	Final	01-07-06 to 28-02-06

4. TITLE AND SUBTITLE
Evaluation of the ISSI S3F Film for Distributed Measurements of Pressure Gradient and Wall-Shear in Water at High Reynolds Number

5a. CONTRACT NUMBER
N00014-05-1-0620

5b. GRANT NUMBER

5c. PROGRAM ELEMENT NUMBER

6. AUTHOR(S)
Arnold Fontaine, Jim Crafton, Sergey Fonov, E. Grant Jones, and Larry Goss

5d. PROJECT NUMBER

5e. TASK NUMBER

5f. WORK UNIT NUMBER

7. PERFORMING ORGANIZATION NAME(S) AND ADDRESS(ES)
Applied Research Lab, Penn State University, PO Box 30, State College, PA, 16804-0030
Innovative Scientific Solutions, Inc., 2766 Indian Ripple Road, Dayton OH 45440

8. PERFORMING ORGANIZATION REPORT NUMBER

9. SPONSORING/MONITORING AGENCY NAME(S) AND ADDRESS(ES)
Ronald Joslin

10. SPONSOR/MONITOR'S ACRONYM(S)
ONR

11. SPONSOR/MONITOR'S REPORT NUMBER(S)

12. DISTRIBUTION/AVAILABILITY STATEMENT
unlimited

DISTRIBUTION STATEMENT A
Approved for Public Release
Distribution Unlimited

13. SUPPLEMENTARY NOTES

14. ABSTRACT
This report documents the results of an assessment study of a new technology for distributed measurements of wall-pressure and wall-shear stress in a hydrodynamic application. The objective of the investigation was to evaluate the ISSI Inc. S3F technology under a range of controlled, laboratory hydrodynamic flow conditions representative of wall shear observed in Naval applications, moderate to high Reynolds number liquid flows. The active element for this sensor is a thin film made of an elastomer with known thickness and shear modulus. The measurement is accomplished by monitoring the surface normal and tangential deformations of the film and then converting these deformation fields into pressure gradient and wall-shear stress. The ability of these films to operate in a liquid boundary layer at high shear load was tested in the twelve inch water tunnel at the Applied Research Laboratory/Penn State University. Quantitative and qualitative measurements of 2-D pressure gradient and wall-shear stress distributions were obtained behind a vortex generator, around two strut end-wall junction models, and in a 2-D canonical turbulent boundary layer. Qualitative analysis of the data indicates that the film responds to the direction and magnitude of the local

15. SUBJECT TERMS

16. SECURITY CLASSIFICATION OF:			17. LIMITATION OF ABSTRACT	18. NUMBER OF PAGES	19a. NAME OF RESPONSIBLE PERSON
a. REPORT	b. ABSTRACT	c. THIS PAGE			Arnold A. Fontaine
u	u	u	uu	23	19b. TELEPHONE NUMBER *(Include area code)* 814-863-1765

Evaluation of the ISSI S3F Film for Distributed Measurements of Pressure Gradient and Wall-Shear in Water at High Reynolds Number

Arnold Fontaine[1], Jim Crafton[2], Sergey Fonov[2], E. Grant Jones[2], and Larry Goss[2]

[1]Applied Research Lab Penn State University PO Box 30 State College, PA 16804-0030	[2]Innovative Scientific Solutions, Inc. 2766 Indian Ripple Road Dayton OH 45440

Abstract: This report documents the results of an assessment study of a new technology for distributed measurements of wall-pressure and wall-shear stress in a hydrodynamic application. The objective of the investigation was to evaluate the ISSI Inc. S3F technology under a range of controlled, laboratory hydrodynamic flow conditions representative of wall shear observed in Naval applications, moderate to high Reynolds number liquid flows. The active element for this sensor is a thin film made of an elastomer with known thickness and shear modulus. The measurement is accomplished by monitoring the surface normal and tangential deformations of the film and then converting these deformation fields into pressure gradient and wall-shear stress. The ability of these films to operate in a liquid boundary layer at high shear load was tested in the twelve inch water tunnel at the Applied Research Laboratory/Penn State University. Quantitative and qualitative measurements of 2-D pressure gradient and wall-shear stress distributions were obtained behind a vortex generator, around two strut end-wall junction models, and in a 2-D canonical turbulent boundary layer. Qualitative analysis of the data indicates that the film responds to the direction and magnitude of the local wall-shear stress and wall-pressure gradient (normal stress) under a wide range of Reynolds numbers. A quantitative comparison of the wall-shear stress measurements from several film formulations with a drag balance was conducted. Softer films, limited to low wall-shear, agreed well for stress values below 50 Pa. The stiffest film showed good repeatability and correctly indicated trend, but measured ~ 25% below the drag balance, This difference may be a film property calibration error. Results of this study indicate that the S3F technology can work in moderate to high Reynolds number hydrodynamic applications. The films provide a spatial distribution of surface stress at a reasonable accuracy that may be as improved. The tests identified several areas for further evaluation and development.

Acknowledgement: This material is based upon work supported by the Office of Naval Research (ONR) and Ron Joslin (the program manager) under Grant No. N00014-05-1-0620.

Disclaimer: Any opinions, findings and conclusions, or recommendations expressed in this publication are those of the authors and do not necessarily reflect the views of the Office of Naval Research.

TABLE OF CONTENTS

LIST OF FIGURES

INTRODUCTION

Background:

The measure of surface shear stress or skin friction is a non-trivial challenge in hydrodynamic applications. It can require the use of expensive mechanical balances, intrusive probes and sensors, or a variety of surface mounted substances. A review of the literature yields a variety of techniques including oil films[1], liquid crystals,[2, 3] thermal sensors[1], an array of MEMS based sensors[4], balance designs[5] and near wall velocity sensors[6,7]. Of these established techniques for shear stress measurements, only liquid crystals or oil films offer non-intrusive and continuous distributions of shear over an area on the surface. Both of these techniques have been utilized in wind and water tunnels with success; however some limitations exist for each technique.

The liquid crystal coating technique[8] is a diagnostic that gives rapid visualization and measurements of surface shear stress magnitude and direction over an entire surface in a continuous, non-intrusive manner. A shear-sensitive liquid crystal coating is applied to the test surface and illuminated by a white light source. The reflected color patterns are recorded using a color video camera. Shear-induced color changes are recorded continuously, with potential time responses on the order of milliseconds. Molecules within a shear-sensitive liquid crystal coating scatter white light as a spectrum of colors, with each color having a different orientation relative to the surface. Under normal illumination, any surface point exposed to a shear vector directed away from the observer exhibits a color change, with the color shift being a function of shear magnitude and direction relative to that observer. Conversely, if the shear vector is directed toward the observer, the coating exhibits no color change and appears as a rust or brown color, independent of shear magnitude and direction. The limitations of this technique include the requirement of multiple viewing angles and the fact that the color change is a function of both shear stress and direction of observation. Some difficulty may be encountered when working with complex geometries.

The oil film[1, 9] technique is well established as a means of measuring shear stress. The technique involves coating a model with a thin film of oil with a known viscosity. The thickness of the oil film is monitored as a function of time and the local shear stress is determined using a relationship between the oil thickness and the applied shear stress. Among the limitations of this technique are slow time response and the need to periodically recoat the model with oil.

Measurements of pressure on aerodynamic models have traditionally used arrays of pressure taps or surface mounted pressure transducers. Non-intrusive and continuous measurements of pressure have been demonstrated using Pressure-Sensitive paint [10] (PSP) on wind tunnel models. PSP is an image-based technique where the luminescent intensity of the coating is a function of the partial pressure of oxygen to which the paint is exposed. While the technique is effective in wind tunnel testing, it is dependent on the compressibility of the working fluid, and therefore can not be used for measurements of pressure in water. Compliant film PSP formulations have been developed for hydrodynamic applications with marginal success at best.[11] The fluorescence intensity of emitted light from a fluorescent dye embedded in the PSP film is proportional to the distance between molecules of one chromophore and an attenuating chromophore embedded at different strata in the PSP film.

In summary, while several non-intrusive image based techniques for measurements of pressure and shear stress have been developed, none have demonstrated quantitative distributed measurements of both pressure and wall-shear stress in water over an area of the surface. The

ISSI S3F film technology is a new technique capable of measuring both pressure gradient (normal stress) and wall-shear stress (skin friction) over a surface in a variety of fluids.

Shear and Stress Sensitive Film

The origin of the Shear and Stress Sensitive Film (S3F) technique began in the early 1990s as a direct method to measure surface shear force[12]. This approach consisted of mounting a thin film made of a flexible elastomer of known thickness (h) and shear modulus (μ) onto a model surface, markers were applied to the film and the model surface and an interference method was used to measure the shear deformation of the film caused by flow. The shearing stress was determined using Hooke's law relating shear to strain. The main drawback of this method is the fact that gradients of the normal component of force, pressure for aerodynamic/hydrodynamic flows, can also create a shear-type displacement of the film and thus, the method will work well only in the absence of normal pressure gradients[13]. The S3F technique therefore, is sensitive to both skin friction and pressure gradient. The potential to produce a single sensor for the measurement of both quantities was recognized by ISSI and has subsequently been under development.

Principal of Operation:

Some insight into the operation of the S3F is gained by considering the simplified response of the film to normal and tangential forces. The response to a normal force is depicted in Figure 1. The film will deform under the normal load but will not compress or yield. The local thickness of the film will be modified by the presence of the load near the point of action. Upon removal of the load, the film will return to its original shape. Maximum surface displacement is a function of the material properties and the applied normal load. Materials are typically formulated to produce deflection of less than 5% of total material thickness under anticipated maximum loading, and can be produced to provide less than 1% deflection. The stressed film thickness is a function of the applied normal force (F_N), the original thickness of the film (h), and its modulus (μ): $h=f(F_N, h, \mu)$.

The film responds to gradients in pressure and not changes in static pressure. This can be a significant advantage for several reasons. First, the sensor is a differential rather than an absolute gauge and thus, can be tuned for applications that require larger or smaller sensitivity. Furthermore, the result is a shear sensor that is insensitive to static pressure changes.

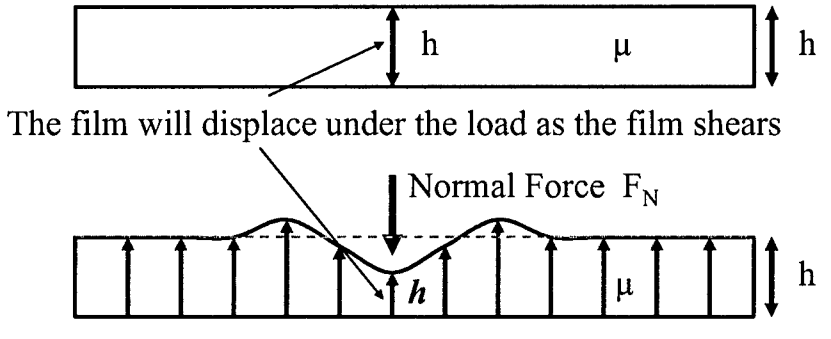

Figure 1: Response of the S3F to a normal load.

The response of the film to a tangential force, F_T, is depicted in Figure 2. Here, the surface of the film will undergo a tangential displacement, D_X, due to the load but again will not yield or compress. The response of the film may be visualized by considering a series of markers on the surface of the film. The markers will be displaced as the film shears and this displacement is a function of the film properties. Again, upon removal of the load the film will return to its original shape. The actual response of the film is more complex as the responses are mildly coupled, a pure tangential load will generate a slight change in film thickness and a pure normal load will generate a slight tangential displacement. These simplified examples however demonstrate the basic operation of the S3F.

One final property of interest is the films frequency response and their potential as a high-frequency probe for both shear stress and pressure. The range of the linear frequency response of such an elastomer is limited by the natural frequency, f_o, of the shear oscillation and can be estimated as

$$f_0 = \frac{1}{2\pi}\sqrt{\frac{\mu}{\rho\, h^2}} \qquad (1)$$

where ρ is the film density. By changing $\mu \in (10 - 1000)$Pa and $h \in (0.1 - 1)$mm, it is possible to adjust the frequency response of the film from 0.3 to 10kHz.

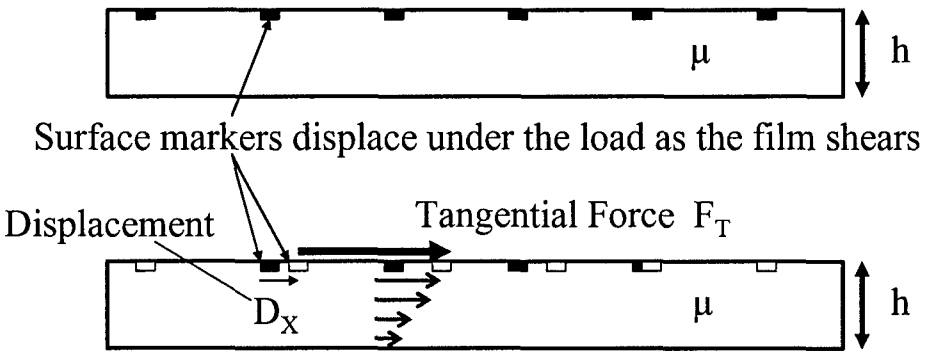

The displacement is a function of the applied force, the thickness of the film, and the shear module of the film

Figure 2: Response of the S3F to a tangential load.

Film Application and Calibration:

In order for a S3F sensor to produce the desired results it must be applied to the surface under study. There are several ways for films to be applied to a surface including spraying with an airbrush, allowing the film to polymerize in a cavity on the model surface, and forming the film in a cavity on a flexible layer which can be glued onto a model surface. Forming films in cavities provides good control of the film thickness and physical properties and control of these parameters is necessary for quantitative measurement of pressure and shear stress. Film formation consists of pouring the polymer components into a flat cavity with a smooth or polished bottom. The film thickness can be estimated by direct measurements using either optical absorption or a capacitive thickness gauge. The film calibration procedure involves applying a

specified load to the film surface and measuring the corresponding normal and tangential deformation of the film.

Measurement System:

The process of measuring pressure and shear is accomplished in two steps. First, the normal and tangential deformation of the film is optically measured. These deformations are then converted to forces using a physical stress/strain model of the film. For these tests, the normal deformation of the film is measured using fluorescence and the tangential deformation is measured using a cross-correlation imaging technique. The experimental setup for this S3F measurement system is presented in Figure 3. All three deformation components can be extracted from a set of flow-off (unloaded) and flow-on (loaded) images taken by a single hi-resolution CCD camera.

The normal component in this configuration is measured using the fluorescence signal emitted from a fluorescent probe embedded in the S3F. Two images are acquired, an unloaded and loaded image, and the ratio of these images is a linear function of film thickness. This type of thickness measurement requires a stable light source and at least a 12-bit CCD camera. The tangential displacement is obtained by spatially cross-correlating the wind-off and wind-on images of the surface providing a two-component deformation map. The surface of the film is lightly doped with small particles that adhere to the surface of the film under load, and do not alter the surface roughness characteristics of the film. This combined fluorescence and cross-correlation procedure was selected for the first generation system because it could be implemented using a single CCD camera.

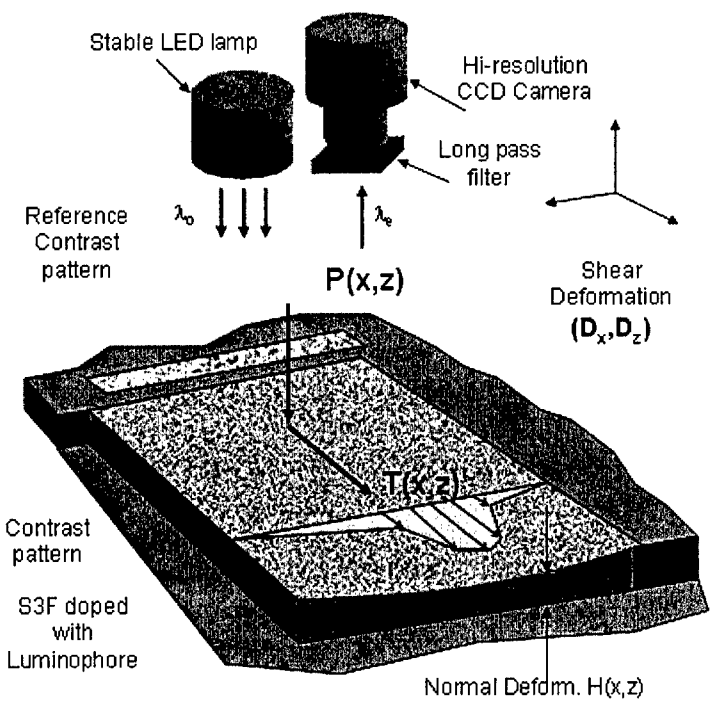

Figure 3: S3F data acquisition system.

Stress Analysis Model for Determination of Forces:

The process of converting deformations to physical stresses is based on a physical stress analysis model of the film. Consider a 1D load applied to the film surface; in this case the film deformation can be treated in 2D space. A rectangular cavity of specified thickness on a plate is filled with an S3F. Constant loads (normal or tangential) are applied to a small region on the film surface. Since the S3F is an elastic solid, it is deformed under the applied force, a point in the solid originally at (x,y) is moved to (X,Y) upon application of the load. If the displacement vector $\vec{r} = (r_1, r_2) = (X - x, Y - y)$ is small, Hooke's law relates the stress tensor σ inside the solid to the deformation (strain) tensor ε [14]:

$$\sigma_{ij} = \lambda \delta_{ij} \nabla . \vec{r} + \mu \varepsilon_{ij}, \quad \varepsilon_{ij} = \frac{1}{2}\left(\frac{\partial r_i}{\partial x_j} + \frac{\partial r_j}{\partial x_i} \right) \tag{2}$$

where δ_{ij} is the Kronecker symbol ($\delta_{ij} = 1$, *if* $i=j$, $\delta_{ij} = 0$, *if* $i \neq j$), and λ, μ are the Lame's constants describing the mechanical properties of the material in terms of the modulus of elasticity E, and Poisson ratio ν

$$\lambda = \frac{E\nu}{(1+\nu)(1-2\nu)}, \quad \mu = \frac{E}{(1+2\nu)} \tag{3}$$

Writing the equation of elasticity in a form for the displacement vector $\vec{r}(x) \in \Omega$ and assuming that no displacement occurs at the boundaries of the cavity (boundary condition).yields:

$$\int_{\Omega} \left[\mu \varepsilon_{ij}(\vec{r}) \varepsilon_{ij}(\vec{w}) + \lambda \varepsilon_{ii}(\vec{r}) \varepsilon_{jj}(\vec{w}) \right] = \int_{\Gamma} \vec{\tau} \cdot \vec{w}, \quad \forall \vec{w} \in \Omega . \tag{4}$$

These integrals are in volume Ω, and on the boundary Γ. In equation (4), $\vec{r}(x)$ is an unknown deformation field and $\vec{w}(x)$ is a test function or virtual deformation field.

To further simplify the physical model of the S3F in Equation (4), the response of the film can be modeled using the response functions of the film to individual normal and tangential loads. The response function of the film to a normal load at the surface, $\delta_n(x)$, includes a normal response function, $\mathbf{n_n(x)}$ and a tangential response function, $\mathbf{n_s(x)}$. Similarly, the response function of the film to a tangential load applied at the surface, $\delta_s(x)$, includes both a normal, $\mathbf{s_n(x)}$, and tangential, $\mathbf{s_s(x)}$, response function. The elastic reaction, $\mathbf{R}(x) \equiv (R_x, R_y)$, can be expressed as the convolution of the response matrix and the applied load components. Assuming that the system is linear, this yields:

$$\mathbf{R}(x) = \int \mathbf{G}(x - x') \, \mathbf{L}(x') \, dx'$$

$$\mathrm{G(x)} = \begin{pmatrix} \mathrm{n_n} & \mathrm{n_s} \\ \mathrm{s_n} & \mathrm{s_s} \end{pmatrix} \quad \text{response matrix} \tag{5}$$

$$\mathrm{L(x)} = \left(\mathrm{L_x}, \mathrm{L_y} \right) \quad \text{applied loads}$$

If the response matrix, **G**(x), can be determined experimentally or by a Finite Element model, the applied loads, **L**(x), can be determined by de-convolution of Equation (5).

$$\mathbf{L} = \mathbf{G}^{-1} \cdot \mathbf{R} \tag{6}$$

Finally, rewriting Equation (5) in a discreet form for the reaction of the film to an arbitrary set of loads applied at discreet surface locations yields:

$$R_{nj} = \Delta x \sum_{k=0}^{N} L_{nk} \tilde{n}_n (x_j - x_k) + L_{gk} \tilde{s}_n (x_j - x_k) \qquad \text{normal reaction}$$

$$R_{sj} = \Delta x \sum_{k=0}^{N} L_{nk} \tilde{n}_s (x_j - x_k) + L_{gk} \tilde{s}_s (x_j - x_k) \qquad \text{tangential reaction} \qquad (7)$$

where $L_j = (L_{nj}, L_{sj})$ are discreet loads

applied at surface locations $x_j = [x_0, x_n]$

This system of linear equations with unknown $\mathbf{L_k}$ has the diagonally dominant matrix

$$G_{jk} = \begin{pmatrix} n_{njk} & s_{njk} \\ n_{sjk} & s_{sjk} \end{pmatrix} \qquad (8)$$

This matrix can be inverted and used to solve for the original loads.

Film Stress Measurement Uncertainty:

The uncertainty in the S3F film measurement technique for estimation of normal and shear stresses is dependent on several factors. The film thickness and modulus governs the amount of surface deformation for an applied load, and controls the frequency response and stability limit (surface wave motion) of the film. These film properties then determine the required spatial resolution needed in the imaging system and define the limit of acceptable surface deformation for the flow under study. A film that produces too much surface deformation can alter the boundary conditions of the flow (smooth to rough surface). The uncertainty in the fluorescence based normal force measurement will be a function of the dye used (temperature sensitivity, quantum yield, signal strength), the bit resolution of the imaging system used to record the fluorescent intensity of the signal, the stability of the light source used to illuminate the dye and the uniformity of the film layer on the surface of the model. Under ideal conditions, ISSI indicates that normal forces can be measured to better than 1% uncertainty. Wind tunnel tests on models of varying shape and size have shown that C_p can be measured to within 5% when compared to a distribution of surface pressure taps.

The shear stress uncertainty is not only dependent on the film properties but also on the imaging system resolution. The technique is a variant of a "PIV" measurement of the surface strain field in the plane of the film. The particles do not move freely and do not vary from frame to frame, thus, image quality of the particle field can be good. Furthermore, the repeatability from image to image can be good providing quality estimates of the mean displacement field with low standard deviation. Stationary targets are embedded in the film and used to quantify and correct for model vibration or displacement independent of the film surface displacement caused by the flow. These film characteristics coupled with the proprietary image processing routines used by ISSI to compute image cross correlation and provide a measure of the surface particle deformation field provide sub-pixel resolution in the estimate of surface strain. In an optimally designed system (properly chosen film modulus and film thickness, high quality imaging, good image resolution, etc.), ISSI indicates that the statistical sub-pixel accuracy of the mean sub-pixel displacement can be as good as 1/20 of a pixel. This estimate is dependent on the number images used in the mean estimate and the level of unsteadiness in the flow producing the surface shear. In a time dependent flow using the high frequency capabilities of the film, the shear stress uncertainty based on a single image pair may be as high as 20% depending on the experimental setup.

EXPERIMENTAL APPROACH

To demonstrate the potential of the S3F for measurements of pressure and shear stress in water under relatively high shear, several experiments were performed in the twelve inch water tunnel at the Applied Research Laboratory (ARL) of Penn State University. These experiments include both qualitative and quantitative measurements of pressure and shear stress over a range of velocities. Experiments were conducted in the two-dimensional test section of the 12-inch diameter water tunnel at ARL/Penn State. The 12 inch tunnel rectangular test section provided an ideal facility to asses the S3F performance in water. Figure 4 provides a schematic of the 12-inch tunnel and a list of the appropriate operating conditions. This test section has a rectangular cross section that measures 508 mm in span by 114 mm in height by 762 mm in length. Turbulence control is through a section of honeycomb in the plenum with a 25 mm core size, 152 mm deep and an 11.3:1 contraction ratio inlet nozzle. The test section turbulence intensity is roughly 0.3-0.5% over the velocity range[15]. The current investigation uses the tunnel wall boundary layer. This side-wall boundary layer has been characterized by two-component LDV and is a canonical, zero pressure gradient, two-dimensional turbulent boundary layer[16].

The flat plate model on which the measurements were made was designed to replace an existing 279 mm by 533 mm test-section window. This plate is mounted flush with the side wall and forms the floating element surface of drag balance assembly. Skin friction drag is measured with a 317.5 mm long by 152.4 mm span drag balance, centered in the tunnel test section. A strain gauged shear flexure is used to measure the skin friction drag force on the wetted surface (flat plate model) of the drag balance. The drag balance is dry calibrated with weights prior to installation in the tunnel. Fontaine et al.[17] describe the balance assembly and its operational characteristics.

Free stream velocity can be accurately controlled and measured over a range from 0 m/s to 19 m/s, with independent control and measurement of the tunnel static pressure at any velocity. The water temperature is continually monitored by a thermistor and can be roughly controlled by draining and refilling the tunnel. The facility has excellent optical access on three sides of the test section with ample room to setup transmitting and receiving hardware for the optical measurements. For these tests, the imaging system, shown in Figure 5, was mounted directly on the top of the test section and S3F samples were mounted on the bottom surface of the test section, as shown in Figure 5. A tent was erected around the test section to limit ambient light.

The quantitative, drag balance tests were conducted in a randomized blind test. The freestream velocity (skin friction) was varied in a random order from zero to maximum velocity for all S3F samples tested. Film deformation images were recorded by ARL staff and sent to ISSI for data processing without identification of the corresponding test parameters. The ISSI processed results were then sent back to ARL for comparison to the known test conditions for each test run. This procedure provides an unbiased estimate of the S3F measured wall-shear for comparison with the known test conditions.

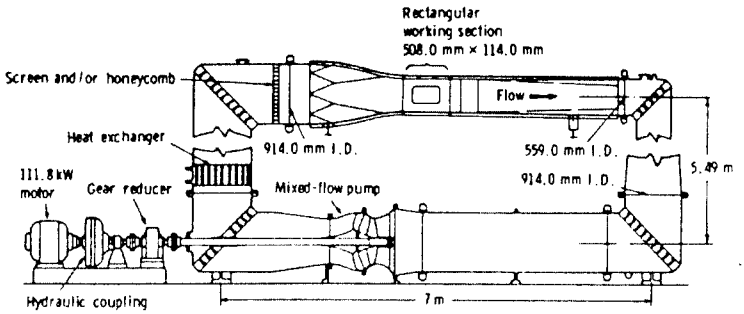

- Closed circuit, closed jet.
- Drive: mixed flow, peerless pump.
- Power: 150 hp.
- Tests:
  - Steady and time dependent operation.
  - Force and pressure measurements.
- Speed: 0 m/s to 21 m/s.
- TI%: < 0.5 %.
- Pressure: 413.7 kPa to 20.7 kPa.
- Cavitation #: > 0.1 dependent on velocity.
- dP/dx = 0 ± 0.25% of total dynamic head.
- Measurement Capabilities:

Figure 4: ARL 12-inch water tunnel.

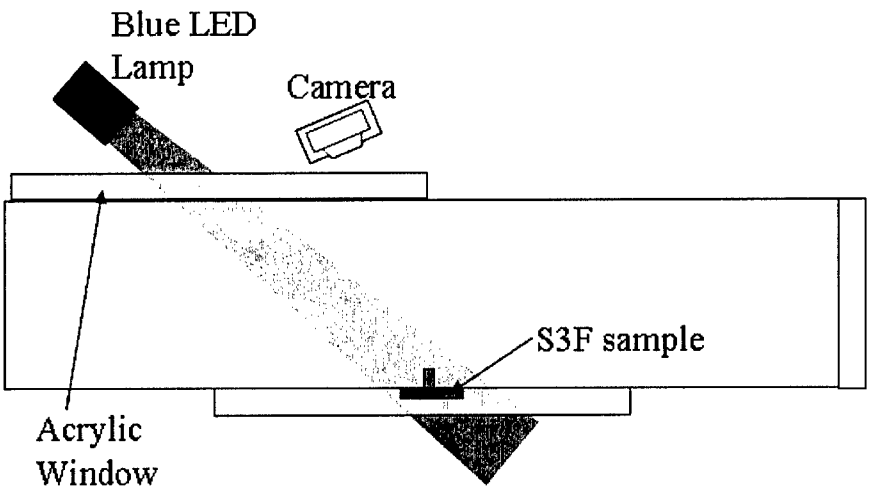

Figure 5: Schematic of Optical setup in 12" tunnel. Flow is out of the plane.

RESULTS

Strut-Endwall Flow

The goal of this test was to demonstrate the ability of the S3F to qualitatively detect shear stresses in water. The selection of the strut-endwall flow is based on the simplicity of the setup as well as the wide recognition of the resulting complex flow field. This flow field includes stagnation points, recirculation zones, and pressure gradients. Two strut-endwall test

configurations were measured. A cylindrical strut with a span that protruded beyond the approach boundary layer, and a shorter, cylindrical strut that had a span of roughly 50% of the approach boundary layer. These two model configurations produce two distinct flow fields. The long strut produces the classic strut-endwall flow field comprised of a stagnation flow, generation of a junction vortex and the downstream separation region. The shorter strut produces a qualitatively similar approach flow but has an altered downstream flow pattern due to the downstream stagnation region generated by the approach boundary deflecting over the cylinder and turning back down toward the wall in the separated flow region downstream. This produces a 3-D flow field qualitatively similar to that produced by flow over a 3-D blunt object. The turbulent boundary thickness at the streamwise location of the plug ranged from 6 to 15 mm depending on free stream velocity.

The strut-endwall tests were conducted by mounting a cylinder along the edge of a 19-mm diameter plug with a 1-mm deep cavity that was filled with S3F. The tests with the short cylinder were conducted with a 3-mm diameter cylinder 5-mm high, centered near one edge of the cavity. The classic strut-endwall tests with the long cylinder were conducted with a 5-mm diameter strut that was approximately 50-mm long. The plug was mounted in the lower wall of the test section with the film downstream of the cylinder and data was acquired at several velocities up to 3.1 m/s using exposure times of 20-ms. For the long cylinder, the plug was then rotated so that the cylinder was located upstream of the film and the test conditions were repeated. Data from the upstream and downstream test configurations can be combined to provide a full representation of the flow around the long strut.

The short strut data are shown in Figure 6 for a tunnel speed of 1.5 m/s. In this case, only the downstream condition was acquired so the image shows the tangential and normal displacement field on the downstream side of the short strut. The vectors represent the magnitude and direction of the tangential displacement field (indicative of shear stress) and the color scale represents the normal displacement field (indicative of pressure gradients). Note, the vectors indicate that the film responds to both the direction and magnitude of the shear stress as evidenced by the data near the downstream stagnation point. In both endwall strut tests, measured pixel displacement varied from sub-pixel displacement in the low shear areas to approximately 1 pixel displacement in the high shear regions of the flows. The vectors depict a separated flow with evidence of a downward directed flow stagnation point as the boundary layer flows up over and around the cylinder. This downward directed flow downstream produces localized increases in wall shear magnitude as the two flow fields (side directed flow around the cylinder and the downward directed flow over the cylinder) merge. The static pressure gradient pattern along the wall is also illustrated in Figure 6 (color contours). The stagnation and the separation regions are clearly depicted in the images. The S3F technique provides a measure of the pressure gradient, and therefore a local pressure measurement in the image field can be used to anchor the gradient measurements and provide a wall static pressure distribution around the model. Tangential and normal displacement values along the centerline (section A-A in Figure 6) are converted to quantitative values of shear stress and pressure, this data is also presented in Figure 6.

The classic strut-endwall test results with the long cylinder are shown in Figure 7. In this case, the upstream and downstream images were combined to produce a composite map of the flow. Again, the tangential displacement field is represented using vectors to show both magnitude and direction, and the color contours represent normal displacements. The location of the upstream junction vortex is apparent in the tangential displacement vectors shown in Figure

7. These contour lines illustrate the curved geometry of the junction vortex as it wraps round the strut and provides an estimate of the upstream displacement of the vortex core from the leading edge of the strut. The low free stream speed produces a large junction vortex that does not tightly wrap around the cylinder as depicted by the direction of the contour lines. The stagnation point is clearly located on the upstream side of the cylinder and regions of increasing shear are present as the flow accelerates around the cylinder. The downstream flow again includes a wall-shear stress stagnation point, however in this case the pressure gradient is relatively flat. This stagnation point is the result of the flow directed around the cylinder merging behind the cylinder. The data along the centerline (section A-A) is converted to quantitative values of pressure and shear stress and are also presented in Figure 7. The locations of the upstream and downstream stagnation points are evident as is the relatively flat pressure gradient. In these figures, $\Delta C_P = (P-P_{ref})/\rho U^2$ where P_{ref} is the free stream pressure (15 psia). The skin friction coefficient is $C_f = 2\tau_W/\rho U^2$. The freestream velocity is U in m/s and τ_W is the wall shear stress.

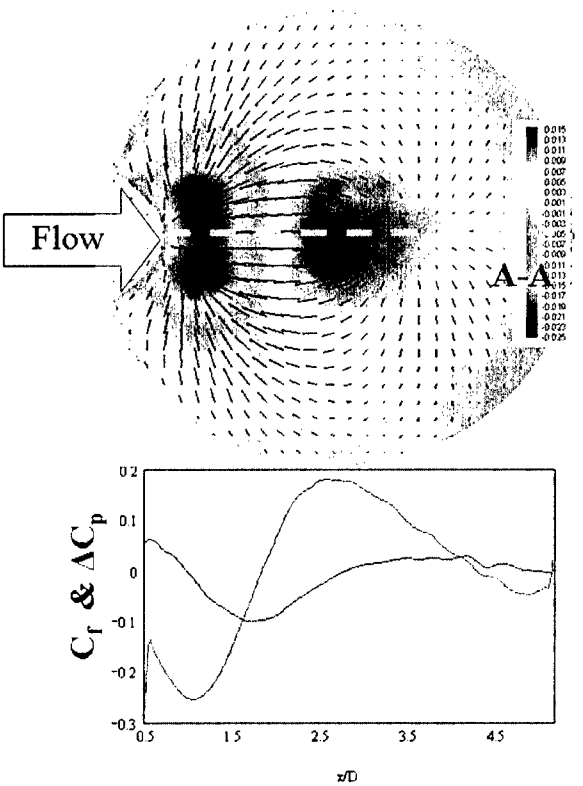

Figure 6: Strut-endwall flow with the short strut.

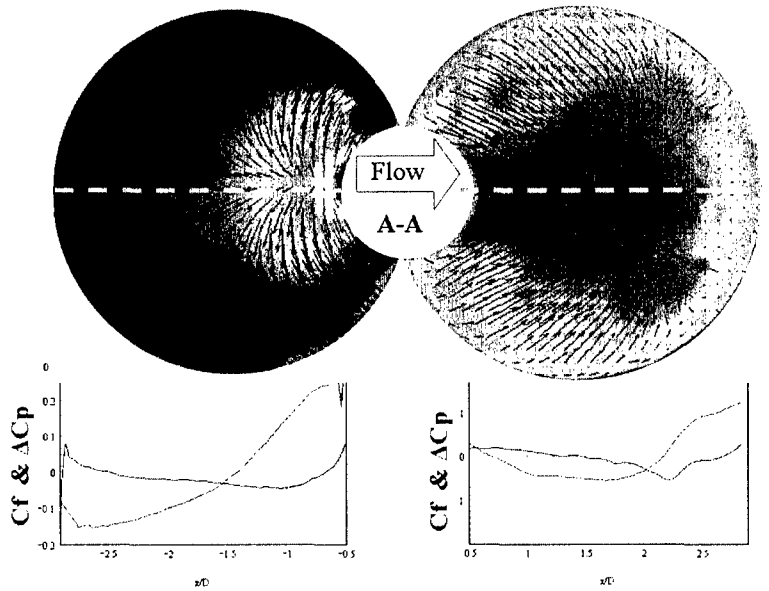

Figure 7: Strut-endwall flow with the long strut.

Pressure and Shear Stress behind a Vortex Generator

The cylinder geometry was replaced with a Delta-wing type vortex generator to further illustrate the ability of the S3F to detect pressure gradients and wall shear patterns generated by secondary flow structures in a boundary layer. The vortex generator flow is of interest for this study due to the one-dimensional structure of the flow. Remember that the model currently used to convert tangential and normal displacements to quantitative pressures and shear stress is based on a one-dimensional linear assumption. The sections selected in Figure 6 and Figure 7 for conversion to quantitative data were chosen because the shear stress along these lines is one-dimensional. The vortex generator flow produces a one-dimensional shear stress field, and therefore the conversion to quantitative values of pressure and shear along several sections should be possible.

A 2-inch by 4-inch cavity of 1-mm depth was filled with S3F and a small vortex generator was positioned on the upstream side of the cavity. Again, data was acquired at several tunnel velocities up to 3.1 m/s. The tangential and normal deformation field for tunnel operation at 1.5 m/s is shown in Figure 8. The presence of the vortex is indicated by the sharp variations in the normal deformation field associated with the pressure gradient from the shed vortex. The color contours show the high pressure field (blue and magenta) caused by the downward directed flow of the vortex on one side with the corresponding low pressure field (yellow and red) on the upwash side of the vortex as illustrated in Figure 8. The scale on the left indicates percent normal deformation of the film, with positive values designating the film is thinner and negative values designating the film is thicker. Quantitative values of pressure and shear are also presented in Figure 8 for three sections downstream of the vertex generator. As expected, the magnitude of the pressure and shear stress disturbance are higher near the trailing edge of the vortex generator. As the vortex convects downstream, viscous dissipation spreads the vortex out creating a wider region of influence but a smaller magnitude of shear stress and pressure. The quantities of C_f and ΔC_p are defined as is Figures 6 and 7.

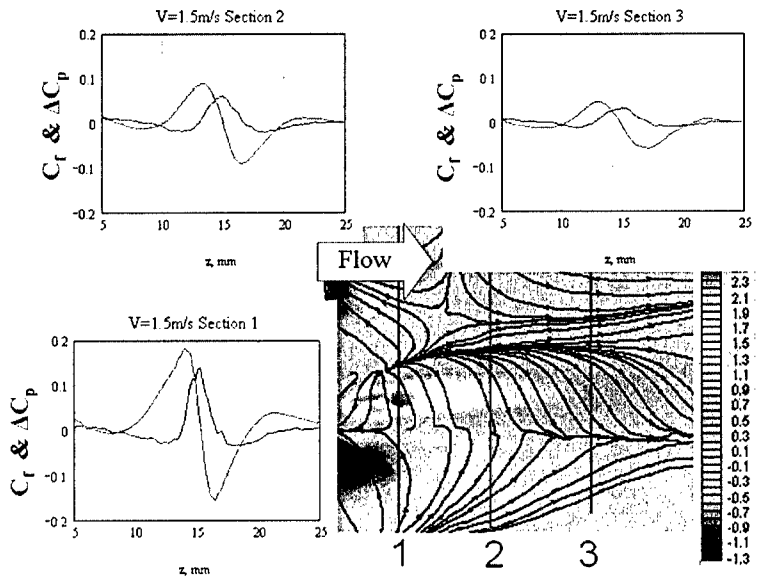

Figure 8: Visualization of the pressure gradient behind a vortex generator.

Wall Shear Stress Measurements Using S3F Plugs

Quantitative measurements of shear stress should be possible with the S3F and these measurements should be repeatable using films of different properties. This was verified by measuring wall shear on the wall of the 12-inch tunnel test section using three S3F samples with differing material properties (stiffness). Several plugs with a cavity diameter of 19-mm and a depth of 1-mm were filled with S3F. Each plug had a S3F with a different shear modulus, varying from 290 Pa to 591 Pa. The plugs were positioned flush with the lower wall of the test section and data were acquired at several velocities from 0.6 m/s to 3.7 m/s. The shear stress measured by the three plugs as function of velocity is presented in Figure 9. Note that while the shear modulus of the film is varied by a factor two, the measured shear stress is relatively constant.

To evaluate the accuracy of the S3F measurements they are compared to experimental measurements of shear stress on a drag balance. Experimental measurements of shear stress were conducted over a range of velocities between 0.75-m/s and 4-m/s using the ARL drag balance and these data points were used to generate a curve for comparison to the S3F data. The S3F data are plotted with the drag balance curve in Figure 9. The S3F data compares favorably with the drag balance measured average shear stress in this velocity range. Unfortunately the films produced for this portion of the test were not stiff enough to withstand higher velocities and could not be tested above 4 m/s without the formation of surface waves. Much of the interest in the ARL water tunnel facility involves higher velocity, and thus higher shear stress environments. While this data can not clearly validate the quantitative aspect of the S3F at the higher velocities, it is concluded that the measurements are repeatable using films of different properties and these measurements compare favorably with experimental measurements of shear stress using a drag balance. The S3F wall-shear stress measurement technique is basically a surface PIV measurement of the surface strain field. As a result, it is sensitive to similar uncertainties in the "particle" displacement measurement. The S3F data presented in Figure 9 represents strain displacements of less than 1 pixel at the lowest velocity to greater than 1 pixel at the higher velocities. The increased error at low velocity may be due to a sub-pixel

displacement uncertainty or resolution effect creating a bias offset in the results. It is possible that the error may also be associated with calibration uncertainty in determining the film properties (thickness and modulus) that are used in the stress analysis model to determine applied load in response to the measured surface deformation.

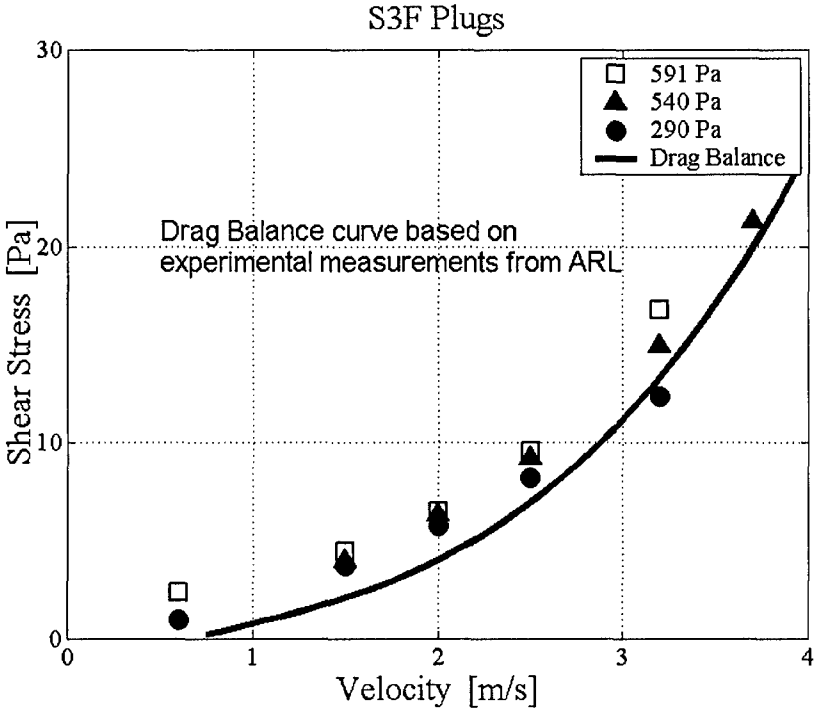

Figure 9: Shear stress measured using three S3F plugs at a range of velocities.

Effect of Static Pressure Changes on S3F

One issue of concern was the effect that static pressure changes would have on the S3F measurement of the surface stress distribution. Theoretically, the film is not compressible and therefore, changes in static pressure should have no effect on measurements of shear stress. In reality, even a slight compressibility of the film could have an impact on shear stress measurements as the magnitude of the pressure force is often several orders of magnitude larger than the magnitude of the shear stress. The 12-inch tunnel provides an excellent environment to test this assumption. The tunnel velocity conditions can remain constant while the tunnel static pressure is varied. The test procedure is based on the assumption that the shear stress is a constant for a given velocity while the static pressure is varied. The data is reduced using a wind-on image at 20-psia as the reference condition, this should allow the effect of static pressure to be evaluated. Assuming that the static pressure has no impact on measurements of pressure gradients and shear stress, the reduced data should show zero tangential and normal deformation.

The 19-mm diameter by 1-mm deep plugs were mounted flush with the tunnel wall. Images of the film were acquired at a tunnel speed of 1.5 m/s while the tunnel static pressure was varied between 10-psia and 30-psia. Reduced data for 15-psia and 30-psia tests are shown in Figure 10. While the normal displacement field is constant, a slight variation in the tangential displacement

field was detected. The tangential displacement field varied over the surface of the plug and the magnitude was approximately 0.1 pixel. Note in Figure 10, the distortion in the tangential field is directed inward when the tunnel is at a higher pressure than the reference condition and outward when the tunnel is at a lower pressure. At this point, these results are considered inconclusive. The distortion in the tangential displacement field may be associated with the imaging system and not the film. Changes in the tunnel static pressure result in distortion or residual stress in the tunnel windows and this could cause slight distortions in the S3F images since the film is imaged through this window. Since the original wind-on image was obtained at a tunnel static pressure of 20 psia, the reversing sign in the measured wall shear stress distributions with varying tunnel static pressure above and below 20 psia may be reasonable if this error is caused by small stress gradients (refractive index gradients) in the window induced by the changes in the pressure loading.

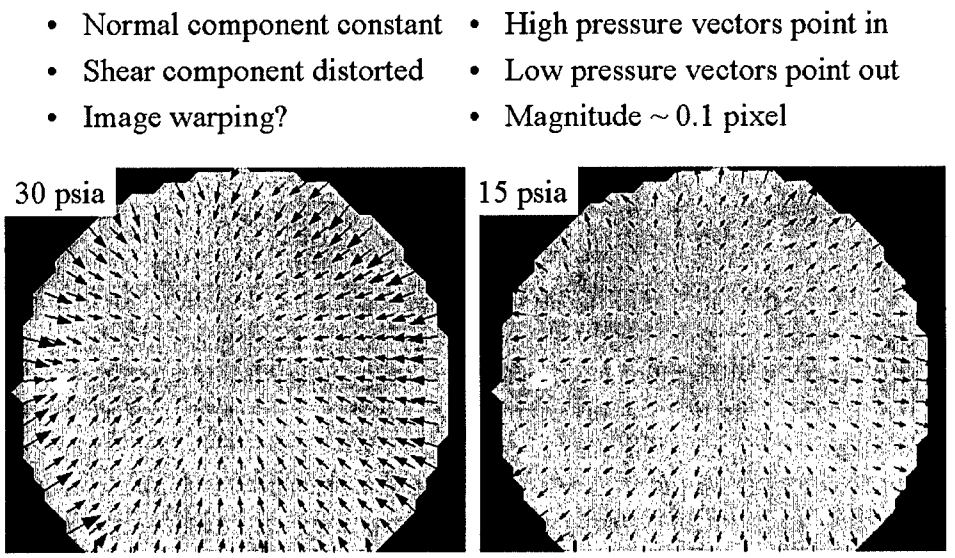

Figure 10: Response of film to changes in static pressure.

It should be noted that the normal force associated with a 5-psi change in static pressure is about 34 KPa while the tangential force is about 30 Pa; a relative magnitude of about 1000. If there is any cross talk between the static pressure and shear stress this effect would be difficult to eliminate here. We believe that the distortion error could be minimized by acquiring a wind-off image at each static pressure. An alternative solution would be to image through windows that have a lower sensitivity to refractive index change with applied load. Regardless of the cause of the variation however, care must be taken to eliminate this source of error from the system.

Wall Shear Stress Measurements Using Stiffer S3F Films

The first entry in the water tunnel provided promising results, however the films produced for this entry were too soft to operate above 4 m/s. To evaluate the S3F for measurements at the higher shear stresses generally encountered in the 12-inch tunnel, a second entry was conducted. The goal of this entry was to make a direct comparison between the shear stress measured by the 12" tunnel large drag balance and that measured by the S3F film with stiffer characteristics suitable for higher shear stress loads. S3F films were applied to an aluminum plate that mounted

onto the tunnel drag balance . The plate included two cavities of 1-mm depth, one cavity was filled with S3F of shear modulus ~ 3.67 KPa and the second cavity contained S3F with a shear modulus of ~ 12.54 KPa. The plate was installed on the balance floating element in the tunnel and images were acquired by ARL staff at a series of tunnel velocities.

These ARL tests were conducted using a short exposure version of a 12-bit PCO Sensicam camera, similar to that used by ISSI but with reduced imaging capability. The ISSI model PCO-1600 camera has a better low light level sensitivity with higher exposure times than the ARL camera, which was limited to less than 10ms exposures. This restricted film imaging to lower f-stops on the camera lens system and produced images of a lower intensity range than those measured in the first phase of the program using the ISSI camera. A 55 mm Nikon-Micro-Nikor macro lens with ~ 12mm of extension between the lens and camera body was used for imaging. Image acquisition was performed using CamWare v2.12 software. The second phase tests used the same ISSI LED lamps used in the first phase of the tests.

These tests were also conducted in a random mode with varying lens f-stop and image acquisition modes to assess hysteresis, and the effects of f-stop and frame averaging. Repeat tests were conducted to assess overall repeatability. Images were acquired at two F-stops, f3.5 and f8, and two acquisition modes, individual frames at 10 ms exposure and frame averaging with 32 frames at 10 ms exposure per frame. Data images, without tunnel velocity or drag balance data, were sent to ISSI for processing in a blind protocol where shear stress measurements were determined and returned to ARL for comparison to the drag balance measurements.

Data was first acquired on the softer of the two films (3.679 KPa) for velocities between 0 and 8.1 m/s. The softer film exhibited surface waves above 8 m/s freestream velocity. The first test followed a random velocity matrix where tunnel velocity was increased and decreased in a random fashion. This provides an assessment of the films ability to respond to changes in velocity and assesses any hysteresis. Figure 11 shows the measured shear stress for the film and balance plotted as a function of run number for two successive runs, the known shear stress for a smooth flat plate curve is included in this figure for comparison. The plate the S3F films were mounted in had leading and trailing edges that were not as flush mounted to the balance floating element as is usually required (approximately 3-5 thousandths high in some areas) and thus, resulted in a slightly higher balance reading than the rigid smooth plate result that was expected. This is indicated by the fact that the drag balance data points are consistently higher than the corresponding Rigid Wall (smooth flat plate) data points in Figure 11, which are consistently measured to within ±3% with this balance when using the ARL smooth wall flat plate floating element module for this balance. The data shown in Figure 11 indicates that an error was observed in the measured shear when the film was loaded beyond 50 Pa. The 50 Pa load condition corresponds to the point where surface waves were observed with this film. It is concluded that this oscillation of the film had the effect of smearing the image of the marker particles on the film surface. This resulted in a loss of a clean correlation peak, and thus inaccurate tangential displacement data. Finally, the issue of hysteresis is addressed by acquiring a zero shear data point at the end of each run. The magnitude of the shear stress measured by the film was consistently below 1.5 Pa indicating that the film exhibits small to negligible hysteresis.

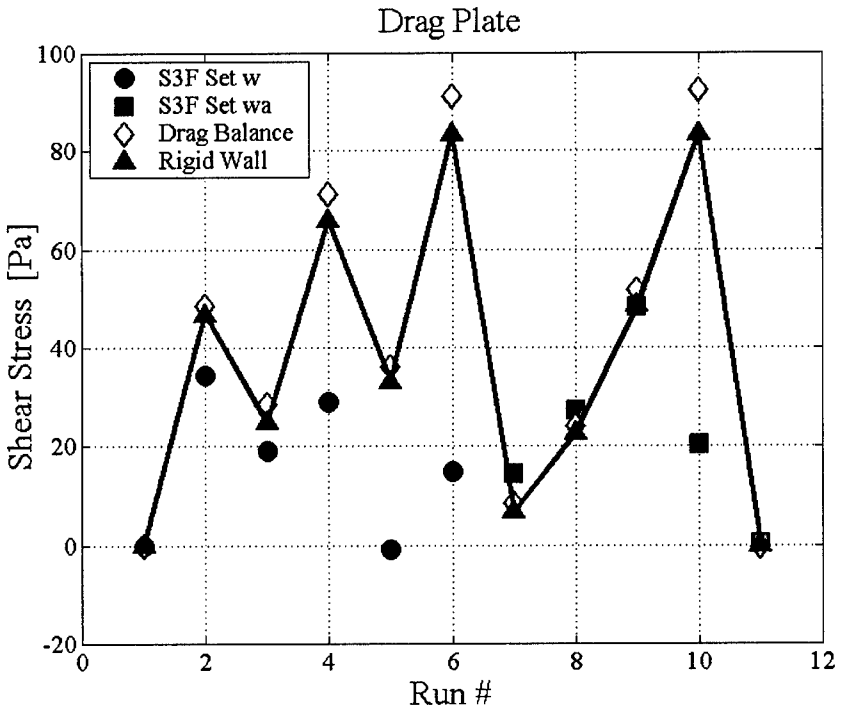

Figure 11: Comparison of measured wall shear between the S3F and balance.

The shear stress measured using the soft film is plotted versus the smooth wall balance reading for three repeats with a lens f-stop of 8 in Figure 12. Perfect agreement would show the S3F data points on the black line in Figure 12. The balance data used in Figure 11 measures roughly 5% higher than expected as explained above, and therefore the smooth wall data from Figure 11 was used in Figure 12 for comparison. Overall, good agreement was obtained for shear stress values below ~50 Pa (6 m/s). As noted above, at higher tunnel velocities the film response does not accurately predict the shear stress. Again, during data acquisition it was noted that the film began to experience a tangential oscillation at higher velocities. It is concluded that this oscillation of the film had the effect of smearing marker particles on the film surface. This resulted in a loss of a clean correlation peak, and thus inaccurate tangential displacement data. Minimizing the oscillation of the film is necessary for shear measurements at higher velocities. The low W1 (open diamond) value (~0 Pa) at the balance measurement of ~32 Pa is the run 5 data point in Figure 11, and is a result of image decorrelation due to tangential oscillations of the film in run 4 as explained above. Disregarding this one point, the agreement is quite good.

Data was next acquired on the stiff (12.54 KPa) film up to 16.1 m/s. The shear stress measured using the stiff film is plotted versus the shear stress measured using the smooth wall data in Figure 13. Data along the black line would indicate agreement between the S3F data and the smooth wall shear correlation. In this Figure, the smooth wall shear correlation is used for comparison since the low shear film started tearing off the plate once the freestream velocity exceeded 11 m/s. The balance measured a progressively higher force at a given velocity as the high shear test progressed due to the cavity forming at the downstream end of the balance section as the low shear film deteriorated. This cavity acted as a severe roughness element to the balance. The cavity disturbance was located more than 15 boundary layer thicknesses downstream of the high shear film located in the middle of the balance plate and therefore,

should have a minimal impact on the measured shear by the high shear film. Since the balance shows better than the 5% agreement with the smooth rigid plate correlation when the S3F film plate was smooth and this error can be attributed to the leading and trailing edge misalignment of the plate, the comparison of the high shear film data to the well-documented smooth rigid plate correlation for this facility is reasonable.

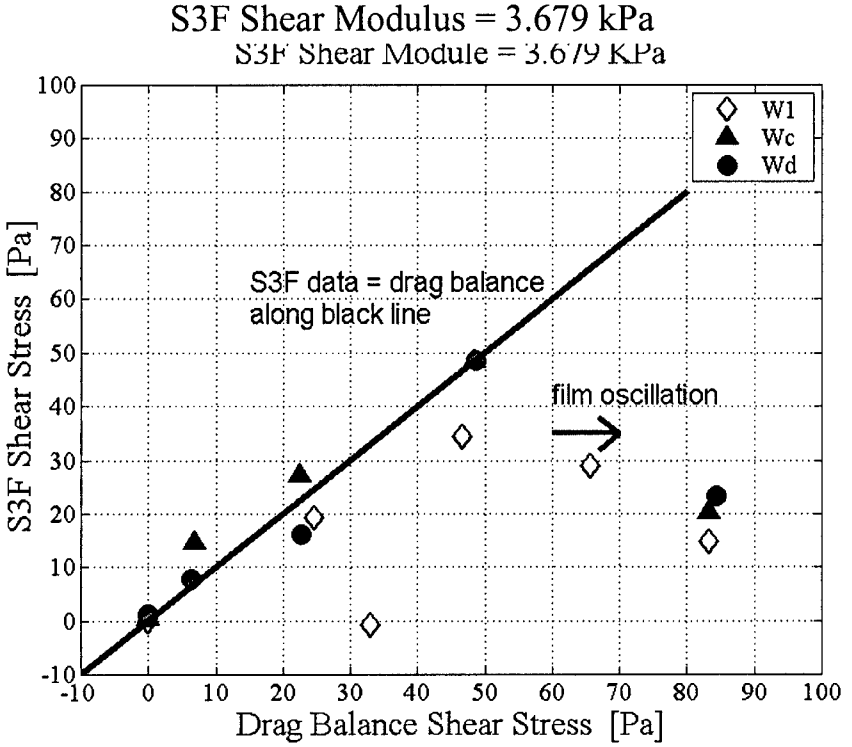

Figure 12: Comparison of shear stress measured using the soft film and drag balance.

It is clear that the stiffer film captured the correct trend throughout the range of velocities however; the magnitude of the S3F measurement is ~ 25% below the smooth plate expected value at the high wall shear stress. It is noted that this film (12.54 KPa) is the stiffest film (by a factor of about 4) that has been produced to date. The technique generally used to determine the shear modulus of the films was not effective for this film and therefore, an auxiliary technique based on an FEA model was applied. It is possible that the error in the shear stress measurements is associated with an incorrect calibration of the shear modulus of the film.

The data shown in Figure 13 suggests that better agreement could be achieved with improved calibration or with the development of an in-situ calibration method. The Wg data set was the last run acquired during this test period. The film had been continually immersed in water for more than 48 hours and was imaged using the averaging modality. It is not clear if the slight difference between the We and Wg data sets are due to the imaging modality or due to possible changes in film properties (modulus or bonding strength at the aluminum interface) with immersion time. Further investigation is recommended to resolve these issues (calibration of stiff films, imaging mode, immersion time or bonding).

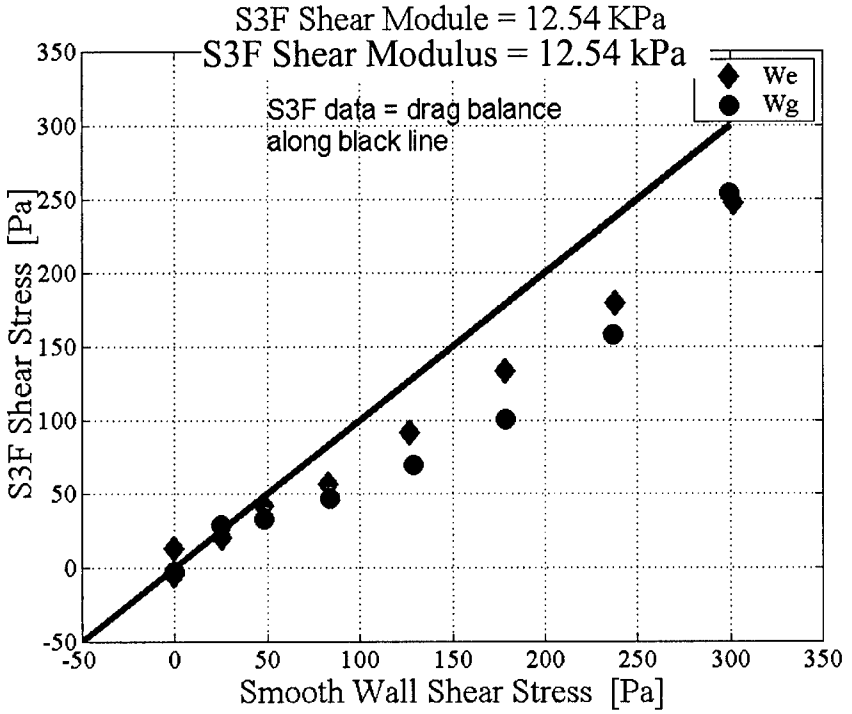

Figure 13: Comparison of shear stress measured using the stiff film and drag balance.

Conclusions

An evaluation test of the S3F film technology has been conducted in the twelve inch water tunnel at the Applied Research Laboratory. Qualitative analysis of the data indicates that the film responds to changes in the direction and magnitude of the local shear stress. Quantitative comparison of the shear stress measurements agreed with measurements from the drag balance to within ±25% over the majority of the test range with increased uncertainty at the lowest wall shear stresses tested. Some of this low shear uncertainty may be due to an image resolution limit similar to that observed in PIV with sub-pixel displacement uncertainty. Increased image magnification or increased CCD chip size (# of pixels) may improve this. Results obtained using the stiffer film modulus, shear modulus 12.5 KPa, display the correct trends but consistently under predict the shear stress by up to 25% above a 50 Pa applied load. This was the stiffest film produced to date. Possible sources of this error may be in the film calibration or in the possibility that adherence properties may have changed in the course of testing at these high wall shear stresses.

In general, accurate wall shear stress measurements can be very difficult with typical uncertainties on the order of ±5%. The best wall shear measurement systems are either single-point, single-measurement devices like hot films or single-measurement, spatially averaging devices like force balances. Overall, the S3F technology shows very promising capability as a wall shear stress sensor in hydrodynamic applications. Its main advantages are the spatial measurement of all **three-components** of the wall stress (two-component wall shear and the normal component related to pressure) applied to a surface and its potential for high frequency response. Pressure gradient is measured as opposed to the local pressure. However, the spatial wall static pressure field as a function of time can be determined by anchoring the measured

pressure gradient distribution with a known pressure measurement by a pressure transducer. It displays very good surface finish, important in high Reynolds number applications, and exhibits good durability under high load. While flat surfaces were the only models coated in this test, the technology should be applicable to curved surfaces or models with complex geometries. The primary requirement is the need for optical access to either the wet surface of the film or from the mounting side of the film. The films can be susceptible to damage if care is not exercised during mounting and installing of test models and surfaces, but this level of care is no more than would be needed for hot films or surface oil applications.

It is suggested that a high quality camera (low light sensitivity, high bit resolution >12-bit, and low noise) is used for the imaging hardware due to the florescence component of the measurement. A stereoscopic (two-camera) system is under development to eliminate the need for fluorescence, but this system increases imaging complexity and optical access requirements for the S3F film system. Since the wall shear stress measurement is essentially a "PIV-type" wall strain measurement, similar problems and concerns that must be addressed in PIV measurements to obtain accurate particle displacement need to be considered here with this technique: camera quality, image quality, number of surface particles, image resolution relative to expected surface displacement, etc. Evaluation of the current data suggests that image focus of the test surface is critical in minimizing measurement error, similar to conventional PIV. The tests conducted with varying f-stop indicate that the higher f-stop images provided better wall-shear estimates and may correlate to improved focus with the higher f-stop. Furthermore, the results comparing frame averaging to the averaging of up to 20 individually acquired frames were inconclusive in identifying whether one method of imaging is better than the other. It is expected that, like in other measurement systems like PIV for example, increasing the number of frames or images used in any statistical estimation of the wall shear will improve overall uncertainty in the estimated value.

The primary limitation of the current system is the assumption of linear behavior in the mathematical modeling that may limit the quantitative accuracy of the films to regions of the flow field exhibiting 2-D behavior. The mathematical inversion model can be extended, though, to more complex scenarios using a full 3-D finite element analysis of the film which is possible with current processing (hardware and software) capabilities. The image processing software currently available with the system would need to be enhanced to perform this analysis. Once developed, it is recommended that follow up tests be conducted to evaluate the quantitative improvement in the estimated value using the more complicated 3-D modeling inversion over that currently obtained with the linear model. Extension to a 3-D modeling approach should provide reasonable quantitative measurements in even complex flows over complex surfaces.

Several unanswered questions remain from this test and should be addressed. The long term stability of the film adhesion to a surface under water needs to be addressed. The short several day test exhibited promising results in this direction. Does exposure to corrosive fluids like sea-water impact film adherence or longevity? Is the film susceptible to environmental fouling, common at sea, or can it be top coated with a thin antifouling membrane? In this study, all the films were applied to the test surfaces in a similar fashion – molded into a cavity. Different application techniques can be used to apply the film, such as spraying, and should be tested for durability and accuracy in the measurement and calibration. The ability to apply the films using a variety of techniques would increase the versatility of the technique to use on complex geometries where cavity molding may not be possible. Finally, an improved calibration technique must be developed for the stiffer films.

REFERENCES

1 Goldstein, Fluid Mechanics Measurements, Taylor & Francis, 1996

2 Reda, D.C., Wilder, M.C., Mehta, R.D., and Zilliac, G. "Measurements of continuous pressure and shear distributions using coating and imaging techniques", AIAA Journal v.36, pp. 895-899, 1998

3 Zhong, S. "Detection of flow separation and reattachment using shear-sensitive liquid crystals", Experiment in Fluids, v.32 pp.667-673, 2002

4 Sheplak, M., Cattafesta, L, Nishida, T., "MEMS Shear Stress Sensors: Promise and Progress", AIAA-2004-2026

5 S. Deutsch, A. A. Fontaine, M. J. Moeny and H. L. Petrie, "Combined Polymer and Microbubble Drag Reduction on a Large Flat Plate," Accepted for Publication, *J. Fluid Mechanics*, 2005.

6 Hochareon, P., Manning, K. B., Fontaine, A., Tarbell, J.M., and Deutsch, S., "Wall shear-rate estimation within the 50cc Penn State Artificial Heart using particle image velocimetry." ASME J Biomech. Eng., 126:430-37, 2004.

7 D. Fourguette, D. Modarress, D. Wilson, M. Koochesfahani, M. Gharib, "An Optical MEMS-Based Shear Stress Sensor for High Reynolds Number Applications",AIAA-03-0742, Reno, Jan 2003.

8 US Patent 5438879.

9 Liu, T, Sullivan, J. "Luminescent oil-film skin friction meter", AIAA journal, Vol. 36, No. 8, pp. 1460-1465, 1998

10 Liu, T, Sullivan, J. "Pressure and Temperature Sensitive Paints", Springer-Verlag, Berlin 2004

11 A. A. Fontaine and H. L. Petrie, "Evaluation of Hydrodynamic Based Pressure sensitive Paint Formulations," ARL Report No. TM 03-038, pp. 1-41, March 2003.

12 Tarasov V.N, Orlov A.A. "Method for determining shear stress on aerodynamic model surface", Patent of Russia, 4841553/23/1990

13 Tarasov V., S. Fonov, A. Morozov, "New gauges for direct skin friction measurements." Proc. Of 17th International Congress on Instrumentation in Aerospace Simulation Facilities (ICIASF), Monterey, California, 29 Sept to 2 Oct 1997

14 Braess, D. "Finite Element", Second Edition, Cambridge University Press, 2001

15 Madavan, N. K., Deutsch, S. and Merkle, C. L., "Reduction of turbulent skin friction by microbubbles," Phys Fluids, 27, 356-363, 1984.

16 Petrie, H. L., Deutsch, S., Brungart, T. A. and Fontaine, A. A., "Polymer drag reduction with surface roughness in flat-plate turbulent boundary layer flow," Exp Fluids, vol 35, pp.8-23, 2003.

17 S. Deutsch, M. J. Moeny, A. A. Fontaine, and H. L. Petrie, "Microbubble Drag Reduction in Rough Walled Turbulent Boundary Layers with Comparison against Polymer Drag Reduction," *Exp. Fluids*, 37(5): 731-44, 2004

Contract Information

Contract Number	N00014-05-1-0620
Title of Research	High Reynolds, Water Tunnel Evaluation of the ISSI S3F Wall-Shear and Surface Pressure Gradient Film Technology
Principal Investigator	Arnold A. Fontaine
Organization	Applied Research Laboratory , Penn State University

Technical Section

Technical Objectives

The measure of surface shear stress or skin friction is a non-trivial challenge in hydrodynamic applications. It can require the use of expensive mechanical balances, intrusive probes and sensors, or a variety of surface mounted substances. A review of the literature yields a variety of techniques including oil films[i], liquid crystals[ii, iii], thermal sensors[i], an array of MEMS based sensors[iv], balance designs[v] and near wall velocity sensors[vi,vii]. Of these established techniques for shear stress measurements, only liquid crystals or oil films offer non-intrusive and continuous distributions of shear over an area on the surface. Both of these techniques have been utilized in wind and water tunnels with success; however some limitations exist for each technique.

The liquid crystal coating technique[viii] is a diagnostic that gives rapid visualization and measurements of surface shear stress magnitude and direction over an entire surface in a continuous, non-intrusive manner. A shear-sensitive liquid crystal coating is applied to the test surface and illuminated by a white light source. The reflected color patterns are recorded using a color video camera. Shear-induced color changes are recorded continuously, with potential time responses on the order of milliseconds. Molecules within a shear-sensitive liquid crystal coating scatter white light as a spectrum of colors, with each color having a different orientation relative to the surface. Under normal illumination, any surface point exposed to a shear vector directed away from the observer exhibits a color change, with the color shift being a function of shear magnitude and direction relative to that observer. Conversely, if the shear vector is directed toward the observer, the coating exhibits no color change and appears as a rust or brown color, independent of shear magnitude and direction. The limitations of this technique include the requirement of multiple viewing angles and the fact that the color change is a function of both shear stress and direction of observation. Some difficulty may be encountered when working with complex geometries.

The oil film[i, ix] technique is well established as a means of measuring shear stress. The technique involves coating a model with a thin film of oil with a known viscosity. The thickness of the oil film is monitored as a function of time and the local shear stress is determined using a relationship between the oil thickness and the applied shear stress. Among the limitations of this technique are slow time response and the need to periodically recoat the model with oil.

Measurements of pressure on aerodynamic models have traditionally used arrays of pressure taps or surface mounted pressure transducers. Non-intrusive and continuous measurements of pressure have been demonstrated using Pressure-Sensitive paint [x] (PSP) on wind tunnel models. PSP is an image-based technique where the luminescent intensity of the coating is a function of the partial pressure of oxygen to which the paint is exposed. While the technique is effective in wind tunnel testing, it is dependent on the compressibility of the working fluid, and therefore can not be used for measurements of pressure in water. The fluorescence intensity of emitted light from a fluorescent dye embedded in the PSP film is proportional to the distance between molecules of one chromophore and an attenuating chromophore embedded at different strata in the PSP film.

In summary, while several non-intrusive image based techniques for measurements of pressure and shear stress have been developed, none have demonstrated quantitative distributed measurements of both pressure and wall-shear stress in water over an area of the surface. The ISSI S3F film technology is a new technique capable of measuring both pressure gradient (normal stress) and wall-shear stress (skin friction) over a surface in a variety of fluids.

Technical Approach

The origin of the Shear and Stress Sensitive Film (S3F) technique began in the early 1990s as a direct method to measure surface shear force[xi]. This approach consisted of mounting a thin film made of a flexible elastomer of known thickness (h) and shear modulus (μ) onto a model surface, markers were applied to the film and the model surface and an interference method was used to measure the shear deformation of the film caused by flow. The shearing stress was determined using Hooke's law relating shear to strain. The main drawback of this method is the fact that gradients of the normal component of force, pressure for aerodynamic/hydrodynamic flows, can also create a shear-type displacement of the film and thus, the method will work well only in the absence of normal pressure gradients[xii]. The S3F technique therefore, is sensitive to both skin friction and pressure gradient. The potential to produce a single sensor for the measurement of both quantities was recognized by ISSI and has subsequently been under development.

Principal of Operation:

Some insight into the operation of the S3F is gained by considering the simplified response of the film to normal and tangential forces. The response to a normal force is depicted in Figure 1. The film will deform under the normal load but will not compress or yield. The local thickness of the film will be modified by the presence of the load near the point of action. Upon removal of the load, the film will return to its original shape. Maximum surface displacement is a function of the material properties and the applied normal load. Materials are typically formulated to produce deflection of less than 5% of total material thickness under anticipated maximum loading, and can be produced to provide less than 1% deflection. The stressed film thickness is a function of the applied normal force (F_N), the original thickness of the film (h), and its modulus (μ): $\boldsymbol{h}=f(F_N, h, \mu)$.

The film responds to gradients in pressure and not changes in static pressure. This can be a significant advantage for several reasons. First, the sensor is a differential rather than an absolute gauge and thus, can be tuned for applications that require larger or smaller sensitivity. Furthermore, the result is a shear sensor that is insensitive to static pressure changes.

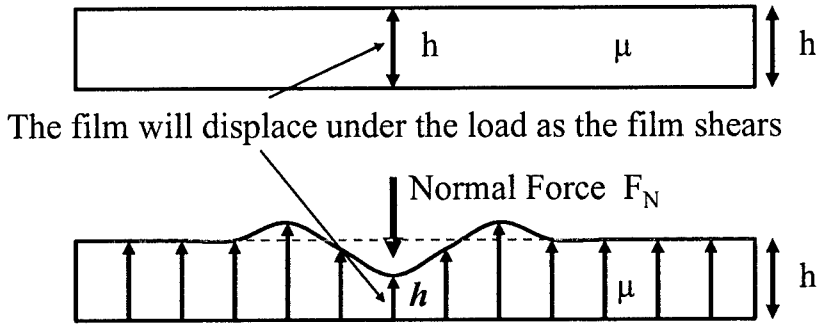

The loaded thickness is a function of the applied force,
the original thickness of the film, and the shear module of the film

Figure 1: Response of the S3F to a normal load.

The response of the film to a tangential force, F_T, is depicted in Figure 2. Here, the surface of the film will undergo a tangential displacement, D_X, due to the load but again will not yield or compress. The response of the film may be visualized by considering a series of markers on the surface of the film. The markers will be displaced as the film shears and this displacement is a function of the film properties. Again, upon removal of the load the film will return to its original shape. The actual response of the film is more complex as the responses are mildly coupled, a pure tangential load will generate a slight change in film thickness and a pure normal load will generate a slight tangential displacement. These simplified examples however demonstrate the basic operation of the S3F.

One final property of interest is the films frequency response and their potential as a high-frequency probe for both shear stress and pressure. The range of the linear frequency response of such an elastomer is limited by the natural frequency, f_o, of the shear oscillation and can be estimated as

$$f_0 = \frac{1}{2\pi}\sqrt{\frac{\mu}{\rho\, h^2}} \qquad (1)$$

where ρ is the film density. By changing $\mu \in (10 - 1000)$Pa and $h \in (0.1 - 1)$mm, it is possible to adjust the frequency response of the film from 0.3 to 10kHz.

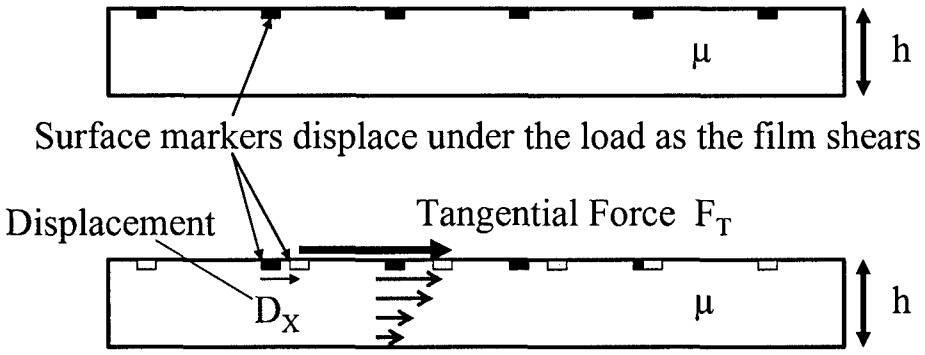

The displacement is a function of the applied force,
the thickness of the film, and the shear module of the film

Figure 2: Response of the S3F to a tangential load.

Film Application and Calibration:

In order for a S3F sensor to produce the desired results it must be applied to the surface under study. There are several ways for films to be applied to a surface including spraying with an airbrush, allowing the film to polymerize in a cavity on the model surface, and forming the film in a cavity on a flexible layer which can be glued onto a model surface. Forming films in cavities provides good control of the film thickness and physical properties and control of these parameters is necessary for quantitative measurement of pressure and shear stress. Film formation consists of pouring the polymer components into a flat cavity with a smooth or polished bottom. The film thickness can be estimated by direct measurements using either optical absorption or a capacitive thickness gauge. The film calibration procedure involves applying a specified load to the film surface and measuring the corresponding normal and tangential deformation of the film.

Measurement System:

The process of measuring pressure and shear is accomplished in two steps. First, the normal and tangential deformation of the film is optically measured. These deformations are then converted to forces using a physical stress/strain model of the film. For these tests, the normal deformation of the film is measured using fluorescence and the tangential deformation is measured using a cross-correlation imaging technique. The experimental setup for this S3F measurement system is presented in Figure 3. All three deformation components can be extracted from a set of flow-off (unloaded) and flow-on (loaded) images taken by a single hi-resolution CCD camera.

The normal component in this configuration is measured using the fluorescence signal emitted from a fluorescent probe embedded in the S3F. Two images are acquired, an unloaded and loaded image, and the ratio of these images is a linear function of film thickness. This type of thickness measurement requires a stable light source and at least a 12-bit CCD camera. The tangential displacement is obtained by spatially cross-correlating the wind-off and wind-on images of the surface providing a two-component deformation map. The surface of the film is

lightly doped with small particles that adhere to the surface of the film under load, and do not alter the surface roughness characteristics of the film. This combined fluorescence and cross-correlation procedure was selected for the first generation system because it could be implemented using a single CCD camera.

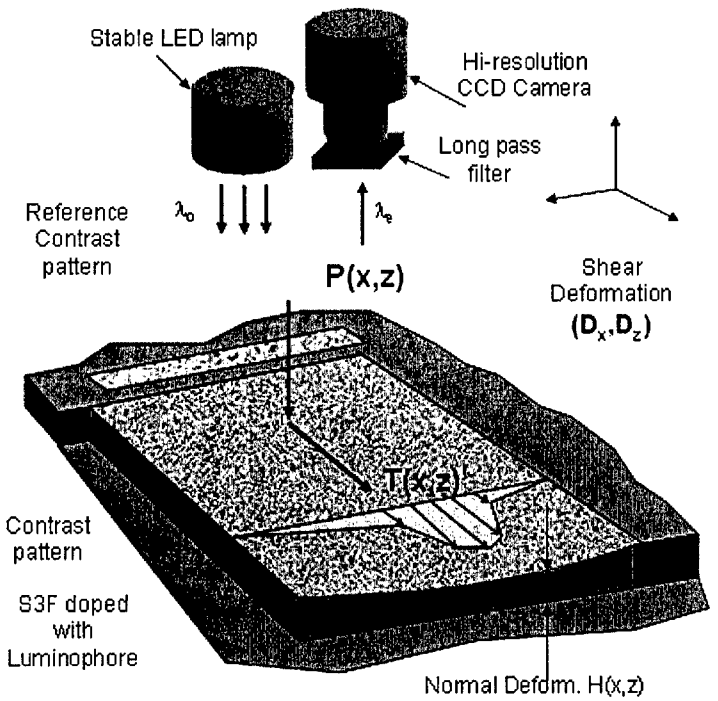

Figure 3: S3F data acquisition system.

Stress Analysis Model for Determination of Forces:

The process of converting deformations to physical stresses is based on a physical stress analysis model of the film. Consider a 1D load applied to the film surface; in this case the film deformation can be treated in 2D space. A rectangular cavity of specified thickness on a plate is filled with an S3F. Constant loads (normal or tangential) are applied to a small region on the film surface. Since the S3F is an elastic solid, it is deformed under the applied force, a point in the solid originally at (x,y) is moved to (X,Y) upon application of the load. If the displacement vector $\vec{r} = (r_1, r_2) = (X - x, Y - y)$ is small, Hooke's law relates the stress tensor σ inside the solid to the deformation (strain) tensor ε [xiii]:

$$\sigma_{ij} = \lambda \delta_{ij} \nabla . \vec{r} + \mu \varepsilon_{ij}, \quad \varepsilon_{ij} = \frac{1}{2}\left(\frac{\partial r_i}{\partial x_j} + \frac{\partial r_j}{\partial x_i} \right) \tag{2}$$

where δ_{ij} is the Kronecker symbol ($\delta_{ij} = 1$, *if* $i=j$, $\delta_{ij} = 0$, *if* $i \neq j$), and λ, μ are the Lame's constants describing the mechanical properties of the material in terms of the modulus of elasticity E, and Poisson ratio ν

$$\lambda = \frac{E\nu}{(1+\nu)(1-2\nu)}, \quad \mu = \frac{E}{(1+2\nu)} \tag{3}$$

Writing the equation of elasticity in a form for the displacement vector $\vec{r}(x) \in \Omega$ and assuming that no displacement occurs at the boundaries of the cavity (boundary condition).yields:

$$\int_{\Omega}\left[\mu\varepsilon_{ij}(\vec{r})\varepsilon_{ij}(\vec{w})+\lambda\varepsilon_{ii}(\vec{r})\varepsilon_{jj}(\vec{w})\right] = \int_{\Gamma}\vec{\tau}\cdot\vec{w}, \quad \forall\vec{w}\in\Omega. \tag{4}$$

These integrals are in volume Ω, and on the boundary Γ. In equation (4), $\vec{r}(x)$ is an unknown deformation field and $\vec{w}(x)$ is a test function or virtual deformation field.

To further simplify the physical model of the S3F in Equation (4), the response of the film can be modeled using the response functions of the film to individual normal and tangential loads. The response function of the film to a normal load at the surface, $\delta_n(x)$, includes a normal response function, $n_n(x)$ and a tangential response function, $n_s(x)$. Similarly, the response function of the film to a tangential load applied at the surface, $\delta_s(x)$, includes both a normal, $s_n(x)$, and tangential, $s_s(x)$, response function. The elastic reaction, $\mathbf{R}(x)\equiv(R_x, R_y)$, can be expressed as the convolution of the response matrix and the applied load components. Assuming that the system is linear, this yields:

$$\mathbf{R}(x) = \int \mathbf{G}(x-x')\,\mathbf{L}(x')\,dx'$$

$$G(x) = \begin{pmatrix} n_n & n_s \\ s_n & s_s \end{pmatrix} \quad \text{response matrix} \tag{5}$$

$$L(x) = \left(L_x, L_y\right) \quad \text{applied loads}$$

If the response matrix, $\mathbf{G}(x)$, can be determined experimentally or by a Finite Element model, the applied loads, $\mathbf{L}(x)$, can be determined by de-convolution of Equation (5).

$$\mathbf{L} = \mathbf{G}^{-1}\cdot\mathbf{R} \tag{6}$$

Finally, rewriting Equation (5) in a discreet form for the reaction of the film to an arbitrary set of loads applied at discreet surface locations yields:

$$R_{nj} = \Delta x\sum_{k=0}^{N} L_{nk}\tilde{n}_n(x_j - x_k) + L_{gk}\tilde{s}_n(x_j - x_k) \quad \text{normal reaction}$$

$$R_{sj} = \Delta x\sum_{k=0}^{N} L_{nk}\tilde{n}_s(x_j - x_k) + L_{gk}\tilde{s}_s(x_j - x_k) \quad \text{tangential reaction} \tag{7}$$

where $L_j = \left(L_{nj}, L_{sj}\right)$ are discreet loads

applied at surface locations $x_j = [x_0, x_n]$

This system of linear equations with unknown $\mathbf{L_k}$ has the diagonally dominant matrix

$$G_{jk} = \begin{pmatrix} n_{njk} & s_{njk} \\ n_{sjk} & s_{sjk} \end{pmatrix} \tag{8}$$

This matrix can be inverted and used to solve for the original loads.

Film Stress Measurement Uncertainty:

The uncertainty in the S3F film measurement technique for estimation of normal and shear stresses is dependent on several factors. The film thickness and modulus governs the amount of surface deformation for an applied load, and controls the frequency response and stability limit (surface wave motion) of the film. These film properties then determine the required spatial resolution needed in the imaging system and define the limit of acceptable surface deformation for the flow under study. A film that produces too much surface deformation can alter the boundary conditions of the flow (smooth to

rough surface). The uncertainty in the fluorescence based normal force measurement will be a function of the dye used (temperature sensitivity, quantum yield, signal strength), the bit resolution of the imaging system used to record the fluorescent intensity of the signal, the stability of the light source used to illuminate the dye and the uniformity of the film layer on the surface of the model. Under ideal conditions, ISSI indicates that normal forces can be measured to better than 1% uncertainty. Wind tunnel tests on models of varying shape and size have shown that C_p can be measured to within 5% when compared to a distribution of surface pressure taps.

The shear stress uncertainty is not only dependent on the film properties but also on the imaging system resolution. The technique is a variant of a "PIV" measurement of the surface strain field in the plane of the film. The particles do not move freely and do not vary from frame to frame, thus, image quality of the particle field can be good. Furthermore, the repeatability from image to image can be good providing quality estimates of the mean displacement field with low standard deviation. Stationary targets are embedded in the film and used to quantify and correct for model vibration or displacement independent of the film surface displacement caused by the flow. These film characteristics coupled with the proprietary image processing routines used by ISSI to compute image cross correlation and provide a measure of the surface particle deformation field provide sub-pixel resolution in the estimate of surface strain. In an optimally designed system (properly chosen film modulus and film thickness, high quality imaging, good image resolution, etc.), ISSI indicates that the statistical sub-pixel accuracy of the mean sub-pixel displacement can be as good as 1/20 of a pixel. This estimate is dependent on the number of images used in the mean estimate and the level of unsteadiness in the flow producing the surface shear. In a time dependent flow using the high frequency capabilities of the film, the shear stress uncertainty based on a single image pair (load on correlated with load off images) may be as high as 20% depending on the experimental setup.

EXPERIMENTAL APPROACH

To demonstrate the potential of the S3F for measurements of pressure and shear stress in water under relatively high shear, several experiments were performed in the twelve inch water tunnel at the Applied Research Laboratory (ARL) of Penn State University. These experiments include both qualitative and quantitative measurements of pressure and shear stress over a range of velocities. Experiments were conducted in the two-dimensional test section of the 12-inch diameter water tunnel at ARL/Penn State. The 12-inch tunnel rectangular test section provided an ideal facility to asses the S3F performance in water. Figure 4 provides a schematic of the 12-inch tunnel and a list of the appropriate operating conditions. This test section has a rectangular cross section that measures 508 mm in span by 114 mm in height by 762 mm in length. Turbulence control is through a section of honeycomb in the plenum with a 25 mm core size, 152 mm deep and an 11.3:1 contraction ratio inlet nozzle. The test section turbulence intensity is roughly 0.3-0.5% over the velocity range[xiv]. The current investigation uses the tunnel wall boundary layer. This side-wall boundary layer has been characterized by two-component LDV and is a canonical, zero pressure gradient, two-dimensional turbulent boundary layer[xv].

The flat plate model on which the measurements were made was designed to replace an existing 279 mm by 533 mm test-section window. This plate is mounted flush with the side wall and forms the floating element surface of drag balance assembly. Skin friction drag is measured with a 317.5 mm long by 152.4 mm span drag balance, centered in the tunnel test section. A strain gauged shear flexure is used

to measure the skin friction drag force on the wetted surface (flat plate model) of the drag balance. The drag balance is dry calibrated with weights prior to installation in the tunnel. Fontaine et al.[xvi] describe the balance assembly and its operational characteristics.

Free stream velocity can be accurately controlled and measured over a range from 0 m/s to 19 m/s, with independent control and measurement of the tunnel static pressure at any velocity. The water temperature is continually monitored by a thermistor and can be roughly controlled by draining and refilling the tunnel. The facility has excellent optical access on three sides of the test section with ample room to setup transmitting and receiving hardware for the optical measurements. For these tests, the imaging system, shown in Figure 5, was mounted directly on the top of the test section and S3F samples were mounted on the bottom surface of the test section, as shown in Figure 5. A tent was erected around the test section to limit ambient light.

The quantitative, drag balance tests were conducted in a randomized blind test. The freestream velocity (skin friction) was varied in a random order from zero to maximum velocity for all S3F samples tested. Film deformation images were recorded by ARL staff and sent to ISSI for data processing without identification of the corresponding test parameters. The ISSI processed results were then sent back to ARL for comparison to the known test conditions for each test run. This procedure provides an unbiased estimate of the S3F measured wall-shear for comparison with the known test conditions.

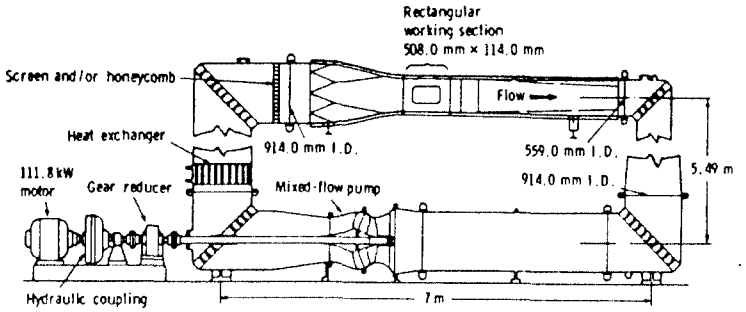

- Closed circuit, closed jet.
- Drive: mixed flow, peerless pump.
- Power: 150 hp.
- Tests:
  - Steady and time dependent operation.
  - Force and pressure measurements.
- Speed: 0 m/s to 21 m/s.
- TI%: < 0.5 %.
- Pressure: 413.7 kPa to 20.7 kPa.
- Cavitation #: > 0.1 dependent on velocity.
- dP/dx = 0 ± 0.25% of total dynamic head.
- Measurement Capabilities:

Figure 4: ARL 12-inch water tunnel.

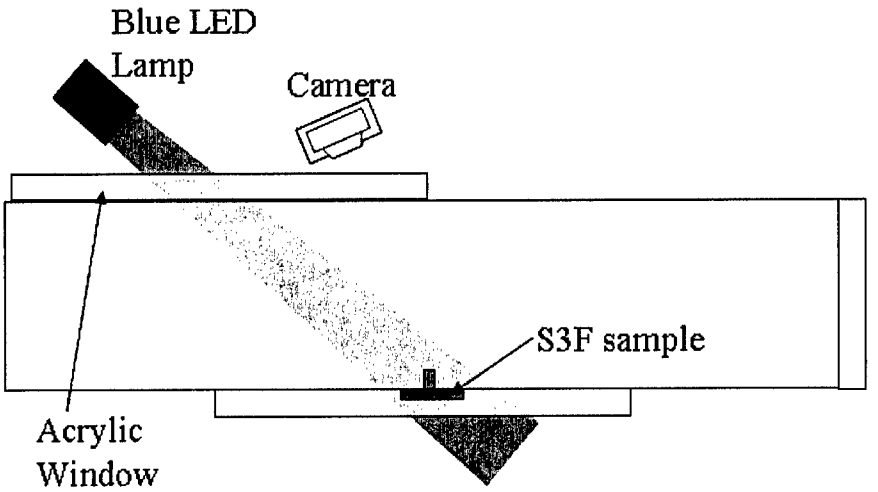

Figure 5: Schematic of Optical setup in 12-inch tunnel; Flow is out of the plane.

Tests conducted with the softer films (strut-endwall, vortex generator, static pressure and low-shear balance tests) in the first phase of the study were performed using a PCO model 1600, 14-bitA/D cooled CCD camera with a 55 mm Nikon lens and 12 mm of extension between the lens and the camera. The balance tests conducted with the stiffer films in the second phase of the study were performed using a short exposure version of a 12-bit PCO Sensicam camera, similar to that used by ISSI but with reduced imaging capability. The PCO-1600 camera has a better low light level sensitivity with higher exposure times than the Sensicam 12-bit camera, which was limited to less than 10ms exposures. This restricted film imaging to lower f-stops on the camera lens system and produced images of a lower intensity range than those measured in the first phase of the program using the softer films. The phase 2 tests used a 55 mm Nikon-Micro-Nikor macro lens with ~ 12mm of extension between the lens and camera body was used for imaging. Image acquisition in phase 2 was performed using CamWare v2.12 software. All tests used the same ISSI LED lamps (model LM2X) which were developed to produce a uniform illumination field with a 400 nm ouput .

RESULTS

Strut-Endwall Flow

The goal of this test was to demonstrate the ability of the S3F to qualitatively detect shear stresses in water. The selection of the strut-endwall flow is based on the simplicity of the setup as well as the wide recognition of the resulting complex flow field. This flow field includes stagnation points, recirculation zones, and pressure gradients. Two strut-endwall test configurations were measured. A cylindrical strut with a span that protruded beyond the approach boundary layer, and a shorter, cylindrical strut that had a span of roughly 50% of the approach boundary layer. These two model configurations produce two distinct flow fields. The long strut produces the classic strut-endwall flow field comprised of a stagnation flow,

generation of a junction vortex and the downstream separation region. The shorter strut produces a qualitatively similar approach flow but has an altered downstream flow pattern due to the downstream stagnation region generated by the approach boundary deflecting over the cylinder and turning back down toward the wall in the separated flow region downstream. This produces a 3-D flow field qualitatively similar to that produced by flow over a 3-D blunt object. The turbulent boundary layer thickness at the streamwise location of the plug ranged from 6 to 15 mm depending on free stream velocity.

The strut-endwall tests were conducted by mounting a cylinder along the edge of a 19-mm diameter plug with a 1-mm deep cavity that was filled with S3F. The tests with the short cylinder were conducted with a 3-mm diameter cylinder 5-mm high, centered near one edge of the cavity. The classic strut-endwall tests with the long cylinder were conducted with a 5-mm diameter strut that was approximately 50-mm long. The plug was mounted in the lower wall of the test section with the film downstream of the cylinder and data was acquired at several velocities up to 3.1 m/s using exposure times of 20-ms. For the long cylinder, the plug was then rotated so that the cylinder was located upstream of the film and the test conditions were repeated. Data from the upstream and downstream test configurations can be combined to provide a full representation of the flow around the long strut.

The short strut data are shown in Figure 6 for a tunnel speed of 1.5 m/s. In this case, only the downstream condition was acquired so the image shows the tangential and normal displacement field on the downstream side of the short strut. The vectors represent the magnitude and direction of the tangential displacement field (indicative of shear stress) and the color scale represents the normal displacement field (indicative of pressure gradients). Note, the vectors indicate that the film responds to both the direction and magnitude of the shear stress as evidenced by the data near the downstream stagnation point. In both endwall strut tests, measured pixel displacement varied from sub-pixel displacement in the low shear areas to approximately 1 pixel displacement in the high shear regions of the flows. The vectors depict a separated flow with evidence of a downward directed flow stagnation point as the boundary layer flows up over and around the cylinder. This downward directed flow downstream produces localized increases in wall shear magnitude as the two flow fields (side directed flow around the cylinder and the downward directed flow over the cylinder) merge. The static pressure gradient pattern along the wall is also illustrated in Figure 6 (color contours). The stagnation and the separation regions are clearly depicted in the images. The S3F technique provides a measure of the pressure gradient, and therefore a local pressure measurement in the image field can be used to anchor the gradient measurements and provide a wall static pressure distribution around the model. Tangential and normal displacement values along the centerline (section A-A in Figure 6) are converted to quantitative values of shear stress and pressure, these data are also presented in Figure 6.

The classic strut-endwall test results with the long cylinder are shown in Figure 7. In this case, the upstream and downstream images were combined to produce a composite map of the flow. Again, the tangential displacement field is represented using vectors to show both magnitude and direction, and the color contours represent normal displacements. The location of the upstream junction vortex is apparent in the tangential displacement vectors shown in Figure

7. These contour lines illustrate the curved geometry of the junction vortex as it wraps around the strut and provides an estimate of the upstream displacement of the vortex core from the leading edge of the strut. The low free stream speed produces a large junction vortex that does not tightly wrap around the cylinder as depicted by the direction of the contour lines. The stagnation point is clearly located on the upstream side of the cylinder and regions of increasing shear are present as the flow accelerates around the cylinder. The downstream flow again includes a wall-shear stress stagnation point, however in this case the pressure gradient is relatively flat. This stagnation point is the result of the flow directed around the cylinder merging behind the cylinder. The data along the centerline (section A-A) are converted to quantitative values of pressure and shear stress and are also presented in Figure 7. The locations of the upstream and downstream stagnation points are evident as is the relatively flat pressure gradient. In these figures, $\Delta C_P = (P-P_{ref})/\rho U^2$ where P_{ref} is the free stream pressure (15 psia). The skin friction coefficient is $C_f = 2\tau_W/\rho U^2$. The freestream velocity is U in m/s and τ_W is the wall shear stress.

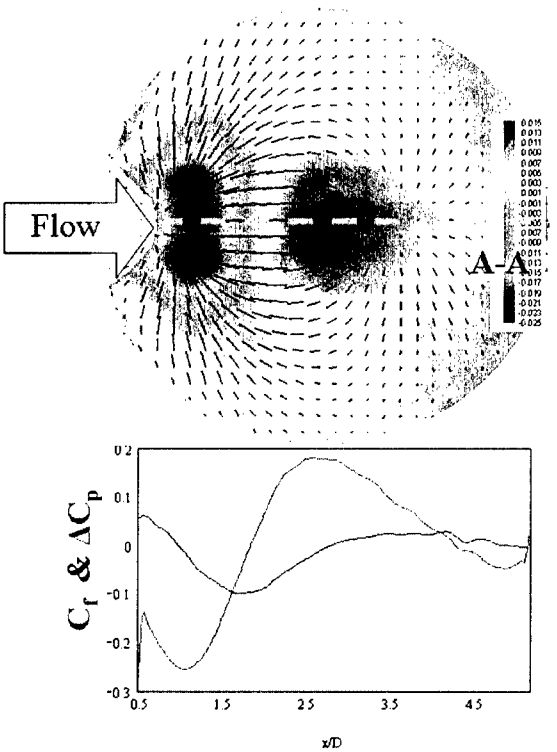

Figure 6: Strut-endwall flow with the short strut.

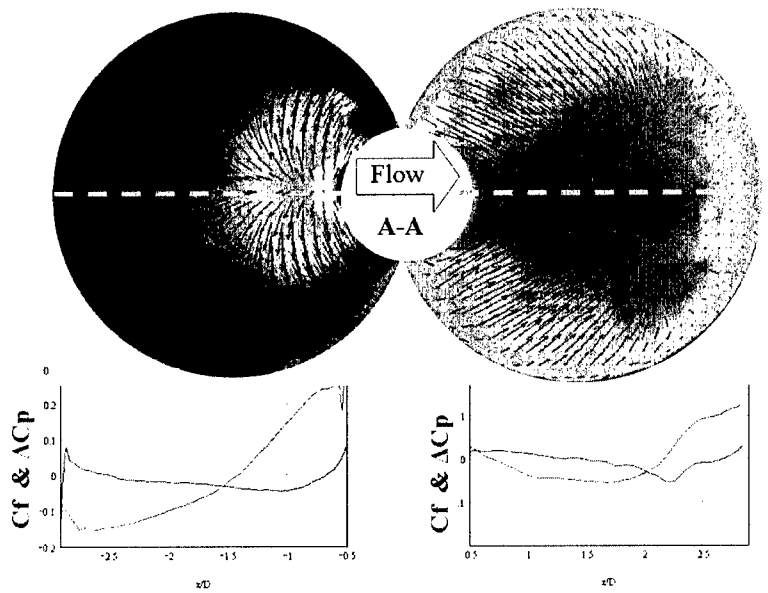

Figure 7: Strut-endwall flow with the long strut.

Pressure and Shear Stress behind a Vortex Generator

The cylinder geometry was replaced with a Delta-wing type vortex generator to further illustrate the ability of the S3F to detect pressure gradients and wall shear patterns generated by secondary flow structures in a boundary layer. The vortex generator flow is of interest for this study due to the one-dimensional structure of the flow. Remember that the model currently used to convert tangential and normal displacements to quantitative pressures and shear stress is based on a one-dimensional linear assumption. The A-A sections selected in Figure 6 and Figure 7 for conversion to quantitative data were chosen because the shear stress along these lines is nearly one-dimensional. The vortex generator flow produces a nearly one-dimensional shear stress field, and therefore the conversion to quantitative values of pressure and shear along several sections should be possible.

A 2-inch by 4-inch cavity of 1-mm depth was filled with S3F and a small vortex generator was positioned on the upstream side of the cavity. Again, data were acquired at several tunnel velocities up to 3.1 m/s. The tangential and normal deformation field for tunnel operation at 1.5 m/s is shown in Figure 8. The presence of the vortex is indicated by the sharp variations in the normal deformation field associated with the pressure gradient from the shed vortex. The color contours show the high pressure field (blue and magenta) caused by the downward directed flow of the vortex on one side with the corresponding low pressure field (yellow and red) on the upwash side of the vortex as illustrated in Figure 8. The scale on the left indicates percent normal deformation of the film, with positive values designating the film is thinner and negative values designating the film is thicker. Quantitative values of pressure and shear are also presented in Figure 8 for three sections downstream of the vortex generator. As expected, the magnitude of the pressure and shear stress disturbance are higher near the trailing edge of the vortex generator. As the vortex convects downstream, viscous dissipation spreads the vortex out

creating a wider region of influence but a smaller magnitude of shear stress and pressure. The quantities of C_f and ΔC_p are defined as is Figures 6 and 7.

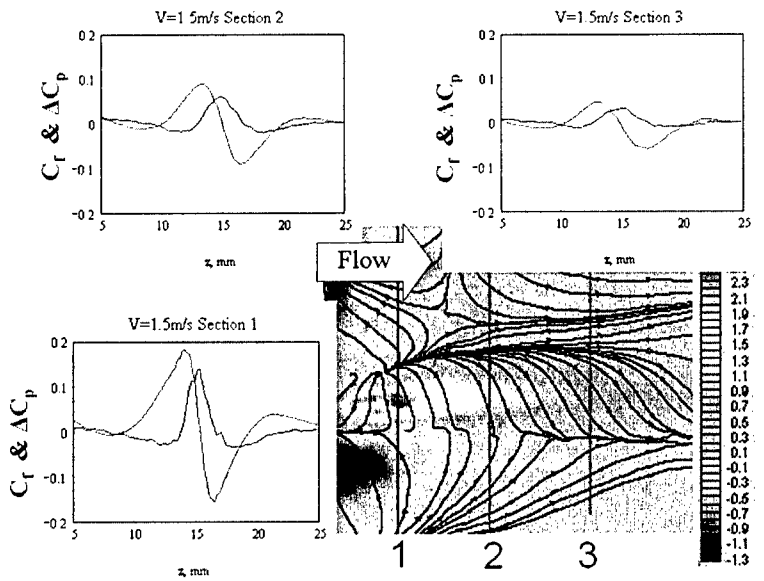

Figure 8: Visualization of the pressure gradient behind a vortex generator.

Wall Shear Stress Measurements Using S3F Plugs

Quantitative measurements of shear stress should be possible with the S3F and these measurements should be repeatable using films of different properties. This was verified by measuring wall shear on the wall of the 12-inch tunnel test section using three S3F samples with differing material properties (stiffness). Several plugs with a cavity diameter of 19-mm and a depth of 1-mm were filled with S3F. Each plug had a S3F with a different shear modulus, varying from 290 Pa to 591 Pa. The plugs were positioned flush with the lower wall of the test section and data were acquired at several velocities from 0.6 m/s to 3.7 m/s. The shear stress measured by the three plugs as function of velocity is presented in Figure 9. Note that while the shear modulus of the film is varied by a factor two, the measured shear stress is relatively constant.

To evaluate the accuracy of the S3F measurements they are compared to experimental measurements of shear stress on a drag balance. Experimental measurements of shear stress were conducted over a range of velocities between 0.75-m/s and 4-m/s using the ARL drag balance and these data points were used to generate a curve for comparison to the S3F data. The S3F data are plotted with the drag balance curve in Figure 9. The S3F data compares favorably with the drag balance measured average shear stress in this velocity range. Unfortunately the films produced for this portion of the test were not stiff enough to withstand higher velocities and could not be tested above 4 m/s without the formation of surface waves. Much of the interest in the ARL water tunnel facility involves higher velocity, and thus higher shear stress environments. While these data can not clearly validate the quantitative aspect of the S3F at the higher velocities, it is concluded that the measurements are repeatable using films of different properties

and these measurements compare favorably with experimental measurements of shear stress using a drag balance. The S3F wall-shear stress measurement technique is basically a surface PIV measurement of the surface strain field. As a result, it is sensitive to similar uncertainties in the "particle" displacement measurement. The S3F data presented in Figure 9 represents strain displacements of less than 1 pixel at the lowest velocity to greater than 1 pixel at the higher velocities. The increased error at low velocity may be due to a sub-pixel displacement uncertainty or resolution effect creating a bias offset in the results. It is possible that the error may also be associated with calibration uncertainty in determining the film properties (thickness and modulus) that are used in the stress analysis model to determine applied load in response to the measured surface deformation.

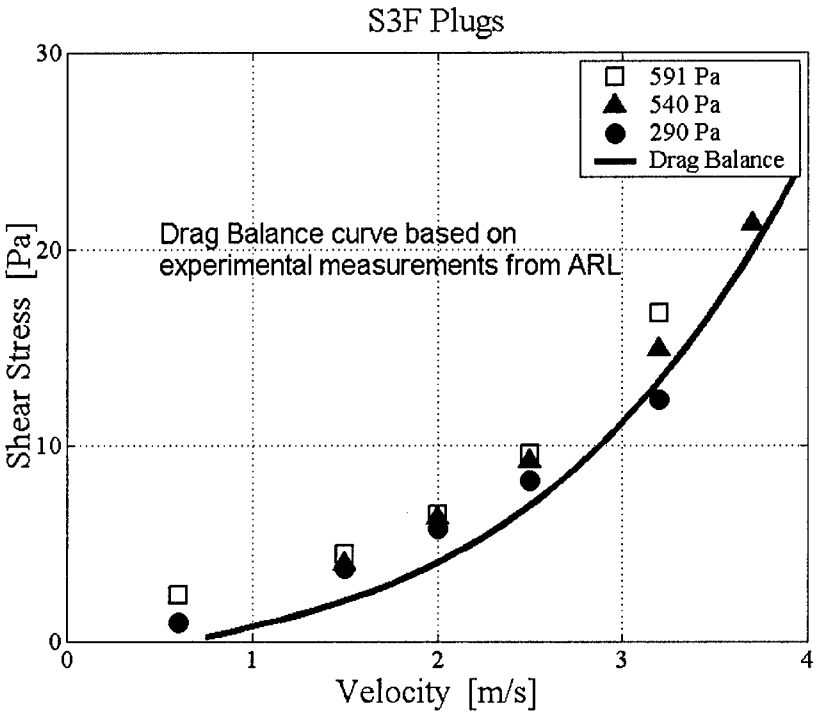

Figure 9: Shear stress measured using three S3F plugs at a range of velocities.

Effect of Static Pressure Changes on S3F

One issue of concern was the effect that static pressure changes would have on the S3F measurement of the surface stress distribution. Theoretically, the film is not compressible and therefore, changes in static pressure should have no effect on measurements of shear stress. In reality, even a slight compressibility of the film could have an impact on shear stress measurements as the magnitude of the pressure force is often several orders of magnitude larger than the magnitude of the shear stress. The 12-inch tunnel provides an excellent environment to test this assumption. The tunnel velocity conditions can remain constant while the tunnel static pressure is varied. The test procedure is based on the assumption that the shear stress is a constant for a given velocity while the static pressure is varied. The data is reduced using a

wind-on image at 20-psia as the reference condition, this should allow the effect of static pressure to be evaluated. Assuming that the static pressure has no impact on measurements of pressure gradients and shear stress, the reduced data should show zero tangential and normal deformation.

The 19-mm diameter by 1-mm deep plugs were mounted flush with the tunnel wall. Images of the film were acquired at a tunnel speed of 1.5 m/s while the tunnel static pressure was varied between 10-psia and 30-psia. Reduced data for 15-psia and 30-psia tests are shown in Figure 10. While the normal displacement field is constant, a slight variation in the tangential displacement field was detected. The tangential displacement field varied over the surface of the plug and the magnitude was approximately 0.1 pixel. Note in Figure 10, the distortion in the tangential field is directed inward when the tunnel is at a higher pressure than the reference condition and outward when the tunnel is at a lower pressure. At this point, these results are considered inconclusive. The distortion in the tangential displacement field may be associated with the imaging system and not the film. Changes in the tunnel static pressure result in distortion or residual stress in the tunnel windows and this could cause slight distortions in the S3F images since the film is imaged through this window. Since the original wind-on image was obtained at a tunnel static pressure of 20 psia, the reversing sign in the measured wall shear stress distributions with varying tunnel static pressure above and below 20 psia may be reasonable if this error is caused by small stress gradients (refractive index gradients) in the window induced by the changes in the pressure loading.

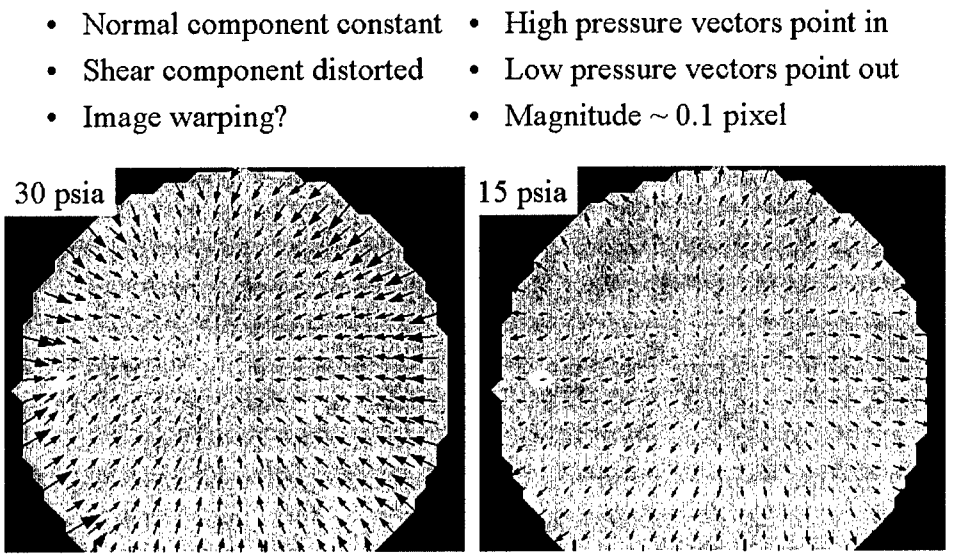

Figure 10: Response of film to changes in static pressure.

It should be noted that the normal force associated with a 5-psi change in static pressure is about 34 KPa while the tangential force is about 30 Pa; a relative magnitude of about 1000. If there is any cross talk between the static pressure and shear stress this effect would be difficult to eliminate here. We believe that the distortion error could be minimized by acquiring a wind-off image at each static pressure. An alternative solution would be to image through windows that

have a lower sensitivity to refractive index change with applied load. Regardless of the cause of the variation however, care must be taken to eliminate this source of error from the system.

Wall Shear Stress Measurements Using Stiffer S3F Films

The first entry in the water tunnel provided promising results, however the films produced for this entry were too soft to operate above 4 m/s. To evaluate the S3F for measurements at the higher shear stresses generally encountered in the 12-inch tunnel, a second entry was conducted. The goal of this entry was to make a direct comparison between the shear stress measured by the 12-inch tunnel large drag balance and that measured by the S3F film with stiffer characteristics suitable for higher shear stress loads. S3F films were applied to an aluminum plate that mounted onto the tunnel drag balance. The plate included two cavities of 1-mm depth, one cavity was filled with S3F of shear modulus ~ 3.67 KPa and the second cavity contained S3F with a shear modulus of ~ 12.54 KPa. The plate was installed on the balance floating element in the tunnel and images were acquired by ARL staff at a series of tunnel velocities.

These ARL tests were conducted using a short exposure version of a 12-bit PCO Sensicam camera, similar to that used by ISSI but with reduced imaging capability. The ISSI model PCO-1600 camera has a better low light level sensitivity with higher exposure times than the ARL camera, which was limited to less than 10ms exposures. This restricted film imaging to lower f-stops on the camera lens system and produced images of a lower intensity range than those measured in the first phase of the program using the ISSI camera. A 55 mm Nikon-Micro-Nikor macro lens with ~ 12mm of extension between the lens and camera body was used for imaging. Image acquisition was performed using CamWare v2.12 software. The second phase tests used the same ISSI LED lamps used in the first phase of the tests.

These tests were also conducted in a random mode with varying lens f-stop and image acquisition modes to assess hysteresis, and the effects of f-stop and frame averaging. Repeat tests were conducted to assess overall repeatability. Images were acquired at two F-stops, f3.5 and f8, and two acquisition modes, individual frames at 10 ms exposure and frame averaging with 32 frames at 10 ms exposure per frame. Data images, without tunnel velocity or drag balance data, were sent to ISSI for processing in a blind protocol where shear stress measurements were determined and returned to ARL for comparison to the drag balance measurements.

Data was first acquired on the softer of the two films (3.679 KPa) for velocities between 0 and 8.1 m/s. The softer film exhibited surface waves above 8 m/s freestream velocity. The first test followed a random velocity matrix where tunnel velocity was increased and decreased in a random fashion. This provides an assessment of the films ability to respond to changes in velocity and assesses any hysteresis. Figure 11 shows the measured shear stress for the film and balance plotted as a function of run number for two successive runs, the known shear stress for a smooth flat plate curve is included in this figure for comparison. The plate the S3F films were mounted in had leading and trailing edges that were not as flush mounted to the balance floating element as is usually required (approximately 3-5 thousandths high in some areas) and thus, resulted in a slightly higher balance reading than the rigid smooth plate result that was expected.

This is indicated by the fact that the drag balance data points are consistently higher than the corresponding Rigid Wall (smooth flat plate) data points in Figure 11, which are consistently measured to within ±3% with this balance when using the ARL smooth wall flat plate floating element module for this balance. The data shown in Figure 11 indicates that an error was observed in the measured shear when the film was loaded beyond 50 Pa. The 50 Pa load condition corresponds to the point where surface waves were observed with this film. It is concluded that this oscillation of the film had the effect of smearing (de-focusing) the image of the marker particles on the film surface. This resulted in a loss of a clean correlation peak, and thus inaccurate tangential displacement data. Finally, the issue of hysteresis is addressed by acquiring a zero shear data point at the end of each run. The magnitude of the shear stress measured by the film was consistently below 1.5 Pa indicating that the film exhibits small to negligible hysteresis.

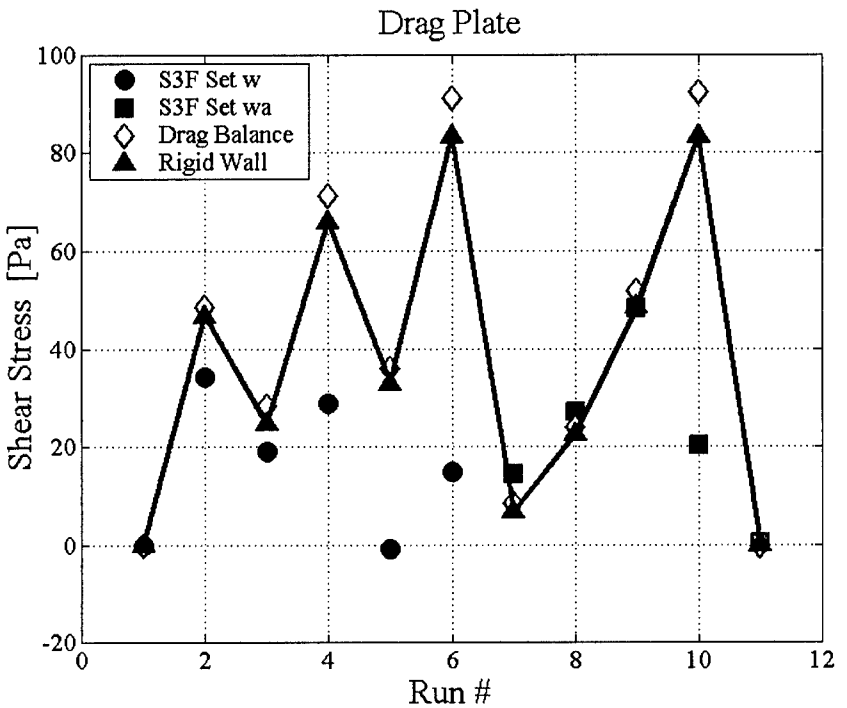

Figure 11: Comparison of measured wall shear between the S3F and balance.

The shear stress measured using the soft film is plotted versus the smooth wall balance reading for three repeats with a lens f-stop of 8 in Figure 12. Perfect agreement would show the S3F data points on the black line in Figure 12. The balance data used in Figure 11 measures roughly 5% higher than expected as explained above, and therefore the smooth wall data from Figure 11 was used in Figure 12 for comparison. Overall, good agreement was obtained for shear stress values below ~50 Pa (6 m/s). As noted above, at higher tunnel velocities the film response does not accurately predict the shear stress. Again, during data acquisition it was noted that the film began to experience a tangential oscillation at higher velocities. It is concluded that this oscillation of the film had the effect of smearing marker particles on the film surface. This

resulted in a loss of a clean correlation peak, and thus inaccurate tangential displacement data. Minimizing the oscillation of the film is necessary for shear measurements at higher velocities. The low W1 (open diamond) value (~0 Pa) at the balance measurement of ~32 Pa is the run 5 data point in Figure 11, and is a result of image decorrelation due to tangential oscillations of the film in run 4 as explained above. Disregarding this one point, the agreement is quite good.

Data was next acquired on the stiff (12.54 KPa) film up to 16.1 m/s. The shear stress measured using the stiff film is plotted versus the shear stress measured using the smooth wall data in Figure 13. Data along the black line would indicate agreement between the S3F data and the smooth wall shear correlation. In this Figure, the smooth wall shear correlation is used for comparison since the low shear film started tearing off the plate once the freestream velocity exceeded 11 m/s. The balance measured a progressively higher force at a given velocity as the high shear test progressed due to the cavity forming at the downstream end of the balance section as the low shear film deteriorated. This cavity acted as a severe roughness element to the balance. The cavity disturbance was located more than 15 boundary layer thicknesses downstream of the high shear film located in the middle of the balance plate and therefore, should have a minimal impact on the measured shear by the high shear film. Since the balance shows better than the 5% agreement with the smooth rigid plate correlation when the S3F film plate was smooth and this error can be attributed to the leading and trailing edge misalignment of the plate, the comparison of the high shear film data to the well-documented smooth rigid plate correlation for this facility is reasonable.

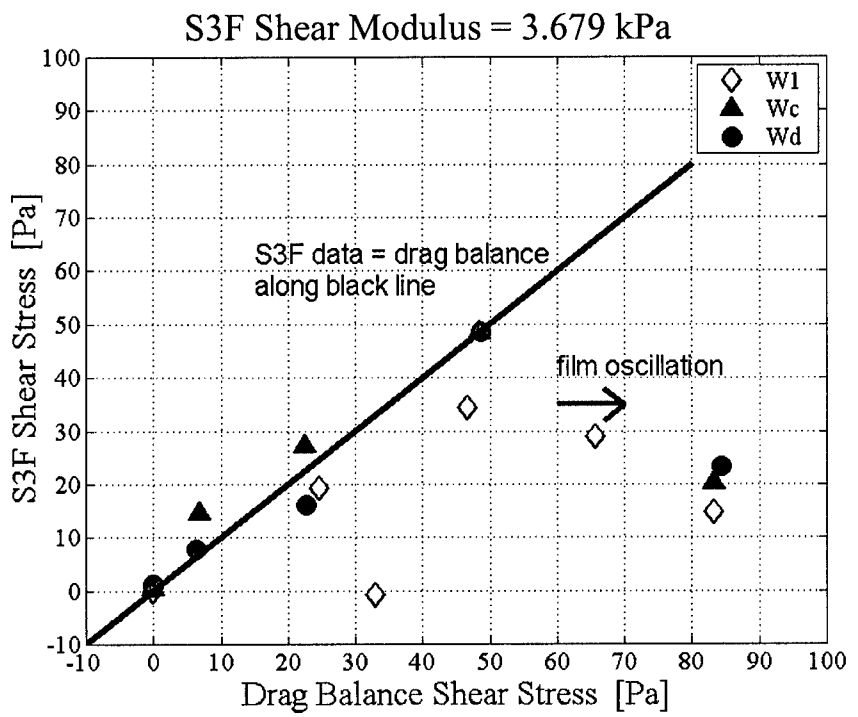

Figure 12: Comparison of shear stress measured using the soft film and drag balance.

It is clear that the stiffer film captured the correct trend throughout the range of velocities however; the magnitude of the S3F measurement is ~ 25% below the smooth plate expected value at the high wall shear stress. It is noted that this film (12.54 KPa) is the stiffest film (by a factor of about 4) that has been produced to date. The technique generally used to determine the shear modulus of the films was not effective for this film and therefore, an auxiliary technique based on an FEA model was applied. It is possible that the error in the shear stress measurements is associated with an incorrect calibration of the shear modulus of the film.

The data shown in Figure 13 suggests that better agreement could be achieved with improved calibration or with the development of an in-situ calibration method. The Wg data set was the last run acquired during this test period. The film had been continually immersed in water for more than 48 hours and was imaged using the averaging modality. It is not clear if the slight difference between the We and Wg data sets are due to the imaging modality or due to possible changes in film properties (modulus or bonding strength at the aluminum interface) with immersion time. Further investigation is recommended to resolve these issues (calibration of stiff films, imaging mode, immersion time or bonding).

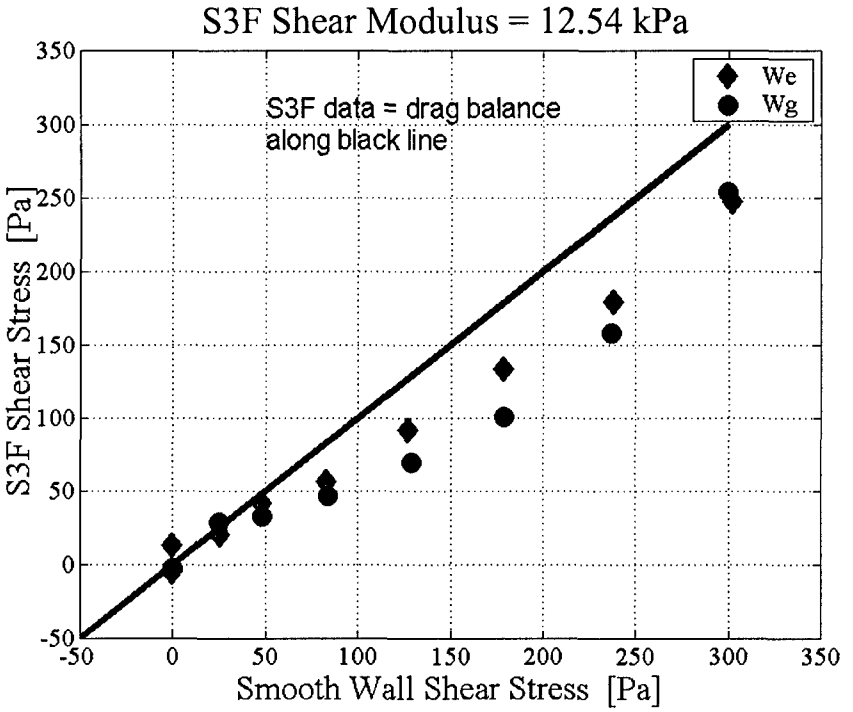

Figure 13: Comparison of shear stress measured using the stiff film and drag balance.

[1] Goldstein, Fluid Mechanics Measurements, Taylor & Francis, 1996.

[1] Reda, D.C., Wilder, M.C., Mehta, R.D., and Zilliac, G. "Measurements of continuous pressure and shear distributions using coating and imaging techniques," *AIAA Journal*, 36:895-9, 1998.

[1] Zhong, S., "Detection of flow separation and reattachment using shear-sensitive liquid crystals," *Experiment in Fluids*, 32:667-73, 2002.

[1] Sheplak, M., Cattafesta, L, and Nishida, T., "MEMS Shear Stress Sensors: Promise and Progress," AIAA-2004-2026.
[1] Deutsch, S., Fontaine, A.A., Money, M.J., and Petrie, H.L., "Combined Polymer and Microbubble Drag Reduction on a Large Flat Plate," Accepted for Publication, *J. Fluid Mechanics*, 2005.
[1] Hochareon, P., Manning, K.B., Fontaine, A.A., Tarbell, J.M., and Deutsch, S., "Wall shear-rate estimation within the 50cc Penn State Artificial Heart using particle image velocimetry," *ASME J Biomech. Eng.*, 126:430-37, 2004.
[1] Fourguette, D., Modarress, D., Wilson, D., Koochesfahani, M., and Gharib, M., "An Optical MEMS-Based Shear Stress Sensor for High Reynolds Number Applications,"AIAA-03-0742, Reno, January 2003.
[1] US Patent 5438879.
[1] Liu, T., and Sullivan, J., "Luminescent oil-film skin friction meter," *AIAA Journal*, 36(8):1460-5, 1998.
[1] Liu, T., and Sullivan, J., "Pressure and Temperature Sensitive Paints," Springer-Verlag, Berlin, 2004.
[1] Tarasov, V.N., and Orlov, A.A., "Method for determining shear stress on aerodynamic model surface," Patent of Russia, **4841553/23**/1990.
[1] Tarasov, V., Fonov, S., Morozov, A., "New gauges for direct skin friction measurements," Proceedings of 17th International Congress on Instrumentation in Aerospace Simulation Facilities (ICIASF), Monterey, California, September 29 through October 2, 1997.
[1] Braess, D. "Finite Element," Second Edition, Cambridge University Press, 2001.
[1] Madavan, N.K., Deutsch, S., and Merkle, C.L., "Reduction of turbulent skin friction by microbubbles," *Phys Fluids*, 27:356-63, 1984.
[1] Petrie, H.L., Deutsch, S., Brungart, T.A., and Fontaine, A.A., "Polymer drag reduction with surface roughness in flat-plate turbulent boundary layer flow," *Exp Fluids*, 35:8-23, 2003.
[1] Deutsch, S., Moeny, M.J., Fontaine, A.A., and Petrie, H.L., "Microbubble Drag Reduction in Rough Walled Turbulent Boundary Layers with Comparison against Polymer Drag Reduction," *Exp. Fluids*, 37(5):731-44, 2004.

Progress

An evaluation test of the S3F film technology has been conducted in the twelve inch water tunnel at the Applied Research Laboratory. Qualitative analysis of the data indicates that the film responds to changes in the direction and magnitude of the local shear stress. Quantitative comparison of the shear stress measurements agreed with measurements from the drag balance to within ±25% over the majority of the test range with increased uncertainty at the lowest wall shear stresses tested. Some of this low shear uncertainty may be due to an image resolution limit similar to that observed in PIV with sub-pixel displacement uncertainty. Increased image magnification or increased CCD chip size (# of pixels) may improve this. Results obtained using the stiffer film modulus, shear modulus 12.5 KPa, display the correct trends but consistently under predict the shear stress by up to 25% above a 50 Pa applied load. This was the stiffest film produced to date. Possible sources of this error may be in the film calibration or in the possibility that adherence properties may have changed in the course of testing at these high wall shear stresses.

In general, accurate wall shear stress measurements can be very difficult with typical uncertainties on the order of ±5%. The best wall shear measurement systems are either single-point, single-measurement devices like hot films or single-measurement, spatially averaging devices like force balances. Overall, the S3F technology shows very promising capability as a wall shear stress sensor in hydrodynamic applications. Its main advantages are the spatial measurement of all **three-components** of the wall stress (two-component wall shear and the normal component related to pressure) applied to a surface and its potential for high frequency response. Pressure gradient is measured as opposed to the local pressure. However, the spatial wall static pressure field as a function of time can be determined by anchoring the measured pressure gradient distribution with a known pressure measurement by a pressure transducer. It displays very good surface finish, important in high Reynolds number applications, and exhibits good durability under high load. While flat surfaces were the only models coated in this test, the technology should be applicable to curved surfaces or models with complex geometries. The primary requirement is the need for optical access to either the wet surface of the film or from the mounting side of the film. The films can be susceptible to damage if care is not exercised during mounting and installing of test models and surfaces, but this level of care is no more than would be needed for hot films or surface oil applications.

It is suggested that a high quality camera (low light sensitivity, high bit resolution >12-bit, and low noise) is used for the imaging hardware due to the florescence component of the measurement. A stereoscopic (two-camera) system is under development to eliminate the need for fluorescence, but this system increases imaging complexity and optical access requirements for the S3F film system. Since the wall shear stress measurement is essentially a "PIV-type" wall strain measurement, similar problems and concerns that must be addressed in PIV measurements to obtain accurate particle displacement need to be considered here with this technique: camera quality, image quality, number of surface particles, image resolution relative to expected surface displacement, etc. Evaluation of the current data suggests that image focus of the test surface is critical in minimizing measurement error, similar to conventional PIV. The tests conducted with varying f-stop indicate that the higher f-stop images provided better wall-shear estimates and may correlate to improved focus with the higher f-stop. Furthermore, the results comparing frame averaging to the averaging of up to 20 individually acquired frames were inconclusive in identifying whether one method of imaging is better than the other. It is expected that, like in other measurement systems like PIV for example, increasing the number of frames or images used in any statistical estimation of the wall shear will improve overall uncertainty in the estimated value.

The primary limitation of the current system is the assumption of linear behavior in the mathematical modeling that may limit the quantitative accuracy of the films to regions of the flow field exhibiting 2-D behavior. The mathematical inversion model can be extended, though, to more complex scenarios using a full 3-D finite element analysis of the film which is possible with current processing (hardware and software) capabilities. The image processing software currently available with the system would need to be enhanced to perform this analysis. Once developed, it is recommended that follow up tests be conducted to evaluate the quantitative improvement in the estimated value using the more complicated 3-D modeling inversion over

that currently obtained with the linear model. Extension to a 3-D modeling approach should provide reasonable quantitative measurements in even complex flows over complex surfaces.

Several unanswered questions remain from this test and should be addressed. The long term stability of the film adhesion to a surface under water needs to be addressed. The short several day test exhibited promising results in this direction. Does exposure to corrosive fluids like sea-water impact film adherence or longevity? Is the film susceptible to environmental fouling, common at sea, or can it be top coated with a thin antifouling membrane? In this study, all the films were applied to the test surfaces in a similar fashion – molded into a cavity. Different application techniques can be used to apply the film, such as spraying, and should be tested for durability and accuracy in the measurement and calibration. The ability to apply the films using a variety of techniques would increase the versatility of the technique to use on complex geometries where cavity molding may not be possible. Finally, an improved calibration technique must be developed for the stiffer films.

---

[i] Goldstein, Fluid Mechanics Measurements, Taylor & Francis, 1996.

[ii] Reda, D.C., Wilder, M.C., Mehta, R.D., and Zilliac, G. "Measurements of continuous pressure and shear distributions using coating and imaging techniques," *AIAA Journal*, 36:895-9, 1998.

[iii] Zhong, S., "Detection of flow separation and reattachment using shear-sensitive liquid crystals," *Experiment in Fluids*, 32:667-73, 2002.

[iv] Sheplak, M., Cattafesta, L, and Nishida, T., "MEMS Shear Stress Sensors: Promise and Progress," AIAA-2004-2026.

[v] Deutsch, S., Fontaine, A.A., Money, M.J., and Petrie, H.L., "Combined Polymer and Microbubble Drag Reduction on a Large Flat Plate," Accepted for Publication, *J. Fluid Mechanics*, 2005.

[vi] Hochareon, P., Manning, K.B., Fontaine, A.A., Tarbell, J.M., and Deutsch, S., "Wall shear-rate estimation within the 50cc Penn State Artificial Heart using particle image velocimetry," *ASME J Biomech. Eng.*, 126:430-37, 2004.

[vii] Fourguette, D., Modarress, D., Wilson, D., Koochesfahani, M., and Gharib, M., "An Optical MEMS-Based Shear Stress Sensor for High Reynolds Number Applications,"AIAA-03-0742, Reno, January 2003.

[viii] US Patent 5438879.

[ix] Liu, T., and Sullivan, J., "Luminescent oil-film skin friction meter," *AIAA Journal*, 36(8):1460-5, 1998.

[x] Liu, T., and Sullivan, J., "Pressure and Temperature Sensitive Paints," Springer-Verlag, Berlin, 2004.

[xi] Tarasov, V.N., and Orlov, A.A., "Method for determining shear stress on aerodynamic model surface," Patent of Russia, **4841553/23**/1990.

[xii] Tarasov, V., Fonov, S., Morozov, A., "New gauges for direct skin friction measurements," Proceedings of 17th International Congress on Instrumentation in Aerospace Simulation Facilities (ICIASF), Monterey, California, September 29 through October 2, 1997.

[xiii] Braess, D. "Finite Element," Second Edition, Cambridge University Press, 2001.

[xiv] Madavan, N.K., Deutsch, S., and Merkle, C.L., "Reduction of turbulent skin friction by microbubbles," *Phys Fluids*, 27:356-63, 1984.

[xv] Petrie, H.L., Deutsch, S., Brungart, T.A., and Fontaine, A.A., "Polymer drag reduction with surface roughness in flat-plate turbulent boundary layer flow," *Exp Fluids*, 35:8-23, 2003.

[xvi] Deutsch, S., Moeny, M.J., Fontaine, A.A., and Petrie, H.L., "Microbubble Drag Reduction in Rough Walled Turbulent Boundary Layers with Comparison against Polymer Drag Reduction," *Exp. Fluids*, 37(5):731-44, 2004.